A one-year ACSM source analysis of organic aerosol particle contributions from anthropogenic sources after long-range transport at the TROPOS research station Melpitz

Samira Atabakhsh[1], Laurent Poulain[1], Gang Chen[2,3], Francesco Canonaco[2,4], André Prévôt[2], Mira Pöhlker[1], Alfred Wiedensohler[1], Hartmut Herrmann[1]

[1]Leibniz Institute for Tropospheric Research, Leipzig, 04318, Germany
[2]Laboratory of Atmospheric Chemistry, Paul Scherrer Institute, Villigen, Aargau, 5232, Switzerland
[3]MRC Centre for Environment and Health, Environmental Research Group, Imperial College London, London, W12 0BZ, U.K.
[4]Datalystica Ltd., Park innovAARE, Villigen, Aargau, 5234,Switzerland

Correspondence to: Hartmut Herrmann (herrmann@tropos.de)

Abstract

Atmospheric aerosol particles are a complex combination of primary emitted sources (biogenic and anthropogenic) and secondary aerosol resulting from aging processes such as condensation, coagulation, and cloud processing. To better understand their sources, investigations have been focused on urban areas in the past, while rural-background stations are normally less impacted by surrounding anthropogenic sources. Therefore, they are predisposed for studying the impact of long-range transport of anthropogenic aerosols. Here, the chemical composition and organic aerosol sources of submicron aerosol particles measured by an aerosol chemical speciation monitor (ACSM) and a multi-angle absorption photometer (MAAP) were investigated at Melpitz from September 2016 to August 2017. The location of the station at the frontier between Western and Eastern Europe makes it the ideal place to investigate the impact of long-range transport over Europe. Indeed, the station is under the influence of less polluted air masses from westerly directions and more polluted continental air masses from Eastern Europe. The OA dominated the submicron particle mass concentration and showed strong seasonal variability ranging from 39 % (in winter) to 58 % (in summer). It was followed by sulphate (15 % and 20 %) and nitrate (24 % and 11 %). The OA source identification was performed using the rolling positive matrix factorisation (PMF) approach to account for the potential temporal changes in the source profile (SoFi Pro). It was possible to split OA into five factors with a distinct temporal variability and mass spectral signature. Three were associated with anthropogenic primary OA (POA) sources: hydrocarbon-like OA (HOA, 5.2 % of OA mass in winter and 6.8 % in summer), biomass burning OA (BBOA, 10.6 %, and 6.1 %) and coal combustion OA (CCOA, 23 %, and 8.7 %). Another two are secondary/processed oxygenated OA (OOA) sources: less-oxidized OOA (LO-OOA, 28.4 %, and 36.7 %) and more-oxidized OOA (MO-OOA, 32.8 %, and 41.8 %). Since equivalent black carbon (eBC) was clearly associated with the identified POA factors (sum of HOA, BBOA, and CCOA, R^2= 0. 87), eBC's contribution to each of the POA factors was achieved using a multi-linear regression model. Consequently, CCOA

34 represented the main anthropogenic sources of carbonaceous aerosol (sum of OA and eBC) not only during winter (56 % of

35 POA in winter) but also in summer (13 % of POA in summer), followed by BBOA (29 % and 69 % of POA in winter and

36 summer, respectively) and HOA (15 % and 18 % of POA in winter and summer, respectively). A seasonal air mass cluster

37 analysis was used to understand the geographical origins of the different aerosol types and showed that during both winter and

38 summer time, PM_1 (PM with an aerodynamic diameter smaller than 1μm) air masses with eastern influence was always

39 associated with the highest mass concentration and the highest coal combustion fraction. Since during winter time, CCOA is

40 a combination of domestic heating and power plants emissions, the summer contribution of CCOA emphasizes the critical

41 importance of coal power plants emissions to rural-background aerosols and its impact on air quality, through long-range

42 transportation.

43 **1 Introduction**

44 Human health effects of air pollution from particulate matter (PM) are well known, and efforts are being made across the world

45 (*WHO, Expert Consultation*, 2019) to minimize both long-term exposures to harmful levels and air pollution peaks. The

46 submicronic particles known as PM_1 (particles with an aerodynamic diameter less than 1 μm), not only have a negative impact

47 on human health (Pop and Dockery, 2016; Daellenbach et al., 2020) but also have a significant effect on visibility (Shi et al.,

48 2014) and climate (Shrivastava et al., 2017). It is ability to penetrate to respiratory system make it more dangerous, therefore

49 more relevant to mitigate adverse health impact. Since the most numerous component of the atmospheric PM is the organic

50 aerosol (OA) (Jimenez et al., 2009; Chen et al., 2022), contributions to OA and explanations of its chemical and physical

51 characteristics remain challenging, whereas the large variety of OA can be attributed to primary emissions by various sources

52 in different seasons, as well as different reactions to atmospheric dynamics and complicated chemical mechanisms depending

53 on meteorological parameters and geographical locations.

54 In order to evaluate and recognize the sources of OA emission, aerosol mass spectrometers (AMS, Jayne et al., 2000) and

55 aerosol chemical speciation monitors (ACSM) (Ng et al., 2011; Fröhlich et al., 2013) are widely deployed worldwide (Chen

56 et al., 2022; Bressi et al., 2021; Fröhlich et al., 2015). AMS is commonly limited to short time periods due to the high

57 maintenance of the AMS measurements and their high operating costs. As a result, only a few studies run AMS continuously

58 (e.g., see Kumar et al., 2022 and O'Dowd et al., 2014). However, there was still a strong need for such a long-term analysis.

59 ACSM is designated for long-term monitoring purposes due to its robustness and much less labour-intense compared to AMS.

60 Therefore, the deployment of ACSM allows us to look at the long-term (more than one year) temporal changes and/or seasonal

61 variability of OA sources.

62 Regarding the identification of OA sources, source apportionment analysis using positive matrix factorisation algorithm (PMF,

63 Paatero and Tappert, 1994) has been intensively used over the past two decades on both AMS and ACSM measurements (e.g.

64 see Crippa et al., 2014; Poulain et al., 2020). However, this algorithm faced two main limitations when used during a long time

65 period: firstly, the factor profiles are static over the analyzing period (Paatero, 1997); and secondly, rotational ambiguity which

provides non-unique solutions. To solve these issues, a multilinear engine (ME-2, Paatero, 1999) has been implemented in the PMF analysis, which allows to use of a priori knowledge to constrain the model to environmentally reasonable solutions (e.g., Canonaco et al., 2013 and Crippa et al., 2014). To consider the temporal variation of the factor profiles, a rolling approach was suggested (Parworth et al., 2015; Canonaco et al., 2020). The rolling strategy involves advancing a smaller PMF window (i.e., 14 days) and moving/rolling it over the whole dataset to catch the temporal changes of the source profiles with a 1-day step. Although several studies in Europe have already conducted source apportionment analyses of one year or more, most of them were associated with urban or suburban environments (e.g., for urban studies: Stavroulas et al., 2019; Vlachou et al., 2019; Huang et al., 2019; Qi et al., 2020; and for suburban studies: Katsanos et al., 2019; Zhang et al., 2019), and only a few of them were studied in rural-background sites (Schlag et al., 2016; Crippa et al., 2014; Vlachou et al., 2018; Paglione et al., 2020; Dudoitis et al., 2016; Heikkinen et al., 2020; Chen et al., 2021; and Chen et al., 2022), although the rural-background sites represent the major advantage to be able to study the impact of long-range transport of anthropogenic emissions and their changes over a long time period. The Leibniz Institute for Tropospheric Research (TROPOS) Central European observatory Melpitz has been continuously measuring aerosol chemical compositions for 30 years. The station is a unique place in Europe, sitting at the border between marine-influenced Western Europe and continental Eastern Europe. A direct consequence is that the aerosol chemical compositions and mass concentrations strongly depend on the air mass origins, showing less polluted air masses coming from the West and more polluted air masses from the East (Birmili et al., 2010; Spindler et al., 2010). However, only a few studies were done on the source identification of the aerosol reaching the station by covering short time periods mostly during winter (van Pinxteren et al., 2016, 2020).

The current study comprehensively investigates the PM_1 aerosol particle chemical compositions and the various OA sources for Melpitz as a rural-background station, based on ACSM and multi-angle absorption photometer (MAAP) measurements from September 2016 to August 2017, using the most advanced rolling PMF with ME-2 implemented in the SoFi Pro package (Datalystica Ltd., Villigen, Switzerland) (Parworth et al., 2015; Canonaco et al., 2013; Canonaco et al., 2020). Although previous papers already considered this dataset, they were focused on quality assurance (Poulain et al., 2020) to depict the European aerosol chemical composition (Bressi et al., 2021 and Chen et al., 2022) or the relationship between the CCN properties (Wang et al., 2022, Schmale et al., 2017), none of these papers were focused on carbonaceous source identification (OA and eBC) nor discussed the strong dependency of the aerosol chemical composition to the air mass origin. Therefore, a multi-linear regression model was used to estimate the contribution of equivalent black carbon (eBC) to the various primary organic PMF factors such as hydrocarbon-like organic aerosol, biomass burning organic aerosol, and coal combustion organic aerosol. Meanwhile, to better understand the emission area of PM_1 chemical composition and PMF factors, the influence of air mass origin was investigated based on self-developed back-trajectory cluster methods (BCLM).

2 Methodology

2.1 Sampling site

The atmospheric aerosol measurements were carried out at the TROPOS research station Melpitz (51.54° N, 12.93° E, 86 m a.s.l.), located approximately 50 km northeast of Leipzig, Germany. The station itself is mainly encircled by agronomical pastures and forests within a rural area, that is why the station is recognized as a rural-background station (Spindler et al., 2013). Since 1992, the station has been monitoring the influence of atmospheric long-range transport on the background air quality of Central European (e.g. Spindler et al., 2012 2013). The Melpitz station is part of EMEP (European Monitoring and Evaluation Programme; Level 3 station, Aas et al., 2012), ACTRIS (Aerosol, Clouds and Trace gases Research Infrastructure), GAW (Global Atmosphere Watch of the World Meteorological Organization), and GUAN (German Ultrafine Aerosol Network, Birmili et al., 2009, 2015, 2016). For a general description of the chemical and physical aerosol characterization analysis techniques, check e.g. Spindler et al., (2004, 2010, 2012, 2013); and Poulain et al., (2011, 2014, 2020).

2.2 ACSM

The chemical compositions and mass loadings of non-refractory PM_1 (NR-PM_1: organic, sulphate, nitrate, ammonium, and chloride) with a 30-minute time resolution were measured by an Aerodyne quadrupole ACSM. The ACSM sampling technique and operational information were previously detailed by Ng et al., (2011).

Briefly, after PM_1 transmits across a 100 μm critical orifice, the aerosols are centralized into a narrow beam in an aerodynamic lens (Liu et al., 2007). Non-refractory particulate material that evaporates at the oven temperature (generally 600°C) is recorded and chemically determined using electron impact quadrupole mass spectrometry at 70 eV (Ng et al., 2011). The ions are then detected using a quadrupole residual gas analyser (RGA, Pfeiffer Vacuum Prisma Plus). The ACSM takes 30-second samples of both ambient and particle-free air. The difference in these measurements identifies the aerosol mass spectrum. To change the signal spectra into organic or inorganic species concentrations, the fragmentation table (Allan et al., 2004), the ion transmission correction, and the Response Factor (RF) are applied. To improve the particle loss as a result of bouncing off the vaporizer, the ACSM data were processed according to manufacturer guidelines using a composition dependent collection efficiency (CDCE) correction relying on the algorithms suggested by Middlebrook et al. (2012). Calibrations of Ionization Efficiency (IE) and Relative Ion Efficiency (RIE) were performed using a 350 nm monodispersed ammonium nitrate and ammonium sulphate (Ng et al., 2011). The final mean value for IE was $4.93(\pm 1.45) \times 10^{-11}$ and the mean values for RIEs for ammonium and sulphate respectively were 6.48 ± 1.26, and 0.68 ± 0.13. The quality assurance of the ACSM measurements was performed by comparing them with collocated measurements including MPSS, and high-volume filter samples (PM_1 and $PM_{2.5}$) for the total particle mass concentration, water-soluble ions (nitrate, sulphate, and ammonium), as well as OC/EC. Details on the QA/QC and instrumental uncertainties can be found in Poulain et al., (2020).

The ACSM ammonium mass concentration mainly corresponds to ammonium nitrate and ammonium sulphate salts. Previously by Poulain et al. (2020), the neutralization state of the particles was estimated for datasets assuming complete neutralization

128 by nitrate, sulphate, and chloride. Therefore, the particles are neutralized when considering nitrate, ammonium, and sulphate

129 in this study. Furthermore, the significant role of organo-nitrate and organo-sulphate on signals of nitrate and sulphate is not

130 negligible (Kiendler- Scharr et al. (2016). Since the Q-ACSM is working at a unit mass resolution (UMR), it is not possible to

131 distinguish nitrate and sulphate from organic. Therefore, estimating the organo-nitrate would only introduce uncertainties to

132 measurements, therefore, we did not consider to conduct this analysis in this study.

133 2.3 Additional measurements

134 In parallel to the ACSM, a MAAP was used to measure the mass concentrations of equivalent black carbon (eBC) (model

135 5012 Thermo Scientific; Petzold and Schönlinner, 2004). The eBC mass concentration from the PM_{10} data was multiplied by

136 a constant factor of 0.9 following Poulain et al (2011) to estimate the eBC mass concentration in the PM_1 fraction.

137 Consequently, all the eBC mass concentrations reported and discussed here correspond to the eBC in the PM_1 fraction and are

138 referred to as eBC-PM_1. Furthermore, a dual mobility particle size spectrometer (TROPOS-type T-MPSS; Birmili et al., 1999)

139 was used to measure the particle number size distribution (PNSD) from 3 to 800 nm (mobility diameter, d mob) at ambient

140 and 300°C temperatures (Wehner et al., 2002). The MAAP was situated in the same laboratory container as the ACSM and

141 these instruments sampled the same PM_{10} inlet after a dryer, and the sampled air distribution among the instruments was

142 equally assured by an isokinetic splitter (Poulain et al., 2020).

143 In addition to the online measurements, high-volume samplers (DIGITEL DHA-80, Digitel Elektronik AG, Hegnau,

144 Switzerland) were utilized to capture daily $PM_{2.5}$ samples on a quartz filter (for 24 hours from midnight to midnight). For more

145 details on the sample preparation and evaluation methods, see Spindler et al., (2013). Levoglucosan as a tracer for wood

146 burning combustion was measured following Iinuma et al., (2009) using high performance anion exchange chromatography

147 coupled with an electrochemical detector (HPAEC-PAD).

148 Trace gas measurements were also carried out. Ozone was determined by a U.V. Photometric gas analyser mode 49C (Thermo

149 Scientific, UK), SO_2 by an APSA-360A (Horiba, Kyoto, Japan), and NO and NO_2 using a customized Trace Level NOx

150 Analysis Model 42i-TL (Thermo Scientific) equipped with a blue light converter. Standard meteorological parameters

151 (temperature, relative humidity, solar radiation, precipitation, wind direction, and wind speed) were regularly measured.

152 2.4 Rolling PMF (ME-2) source apportionment of OA

153 This work conducted the most advanced source apportionment analysis following a standardized protocol developed by Chen

154 et al., (2022). The PMF method was used to allocate the source of the OA (Paatero and Tappert, 1994) through the Source

155 Finder professional (SoFi Pro, version 8.0.3.1, Canonaco et al., 2021) software package (Datalystica Ltd., Villigen,

156 Switzerland), within the Igor Pro software environment (Igor Pro, version 8.04, Wavemetrics, Inc., Lake Oswego, OR, USA).

157 Two matrices of factor profiles *F* and factor contributions *G*, defined the dataset *X*, and the matrix *E* named the residual matrix

158 is the fraction which cannot be described by the model. Time series and the chemical fingerprint of sources have been

159 represented by F_{kj} and G_{ik}, respectively. The dimension of F_{kj} and G_{ik} are based on the order p, which is the number of factors

160 selected to represent the data defined by the user:

161

162 $$X_{ij} = \sum_{k=1}^{p} G_{ik} \times F_{kj} + E_{ij} \qquad (1)$$

163

164 In this study, since the measurement covers a period of 12 months (full four seasons), four separate PMF inputs were prepared.

165 Unconstrained PMF was applied with 4 to 6 factor runs for all the seasons; throughout the pre-result and while referring to

166 previous studies (Crippa et al., 2014 and van Pinxteren et al., 2016) primary factors were separated as hydrocarbon-like OA

167 (HOA), biomass burning OA (BBOA) and coal combustion OA (CCOA). However, unconstrained PMF did not result to

168 separate the primary factor profiles. Introducing constraints based on prior knowledge is an efficient strategy for avoiding the

169 mixing of primary factors (Canonaco et al., 2013; Crippa et al., 2014). For this reason, the multilinear engine (ME-2) algorithm

170 (Paatero, 1999) enables the incorporation of time series and factor profiles constraints in form of the *a*-value approach. In

171 dealing with a profile constraint, the *a-value* specifies the variety of a factor that can deviate from the anchor profile during

172 the PMF iteration:

173 $$f_{j,solution} = f_j \pm a \cdot f_j \qquad (2)$$

174 The constraints applied through ME-2 for HOA and BBOA sources used the anchor profile of Crippa et al., (2014), and Ng et

175 al., (2010), respectively. The anchor profile used for CCOA was generated from our own winter data during this work (SI,

176 1.1). For each of the four seasons, primary profiles were subject to a sensitivity analysis with *a-values* ranging from 0-0.4 for

177 HOA and BBOA, 0-0.5 for CCOA, and steps of 0.1 to choose the best *a-value* combination for these three factors.

178 In the PMF approach, there is the intrinsic property of static factor profiles during the period of PMF analysis. Even though

179 for short-term measurements (like one/two season/s) this might be a sensible estimation, long-term observations as are typical

180 for current ACSM study (one year and more), are expected to be subject to evolving factor profiles based on seasonality. To

181 consider the temporal changes, the rolling PMF window method was developed (Canonaco et al., 2021b; Parworth et al., 2015).

182 This technique is applied to a small window, which is slowly extended throughout the whole dataset. Based on the dataset, the

183 user determines the width of the PMF window, the shift parameter, and the number of PMF repeats per window; for the current

184 work, we set 14-day windows, 1-day shifts, and 100 repeats per window.

185 In addition, this rolling PMF analysis was coupled with the bootstrap re-sampling approach (*Bootstrap Methods: Another Look*

186 *at the Jackknife on JSTOR*, 1979), which can randomly select a part of the original matrix and repeat a part of the rows to

187 generate a new same-sized matrix to test the stability of solutions and to estimate the statistical error. Overall, we have

188 combined rolling PMF with ME-2 and bootstrap to conduct the source apportionment investigation, and more information on

189 this new approach was described in Canonaco et al., (2020). This approach for a yearlong dataset generates an enormous

190 amount of PMF runs (N= 35800) and not all of the solutions are environmentally reasonable. Since it is practically impossible

191 to manually inspect all PMF runs, the criterial-base selection was introduced in SoFi Pro to automatically and objectively

192 select environmentally reasonable PMF solutions (Canonaco et al., 2020). Finally, the resulting factors were interpreted as
193 HOA, BBOA, CCOA, and two oxidized OA (OOA) factors named less-oxygenated OOA (LO-OOA) and more oxygenated
194 OOA (MO-OOA). The steps and setups utilized in the evaluation of this dataset are detailed in the supplement (Sect. 1).

2.5 eBC-PM$_1$ source apportionment

196 The eBC-PM$_1$ correlated with each of the three identified primary organic factors (HOA, BBOA, and CCOA) during the source
197 apportionment analysis (Table. 1, which will be discussed later on in the result Sect.). The total amount of these primary factors
198 (known as POA) was highly correlated with eBC-PM$_1$ (R^2= 0.87; Fig. 8a). As a result, the different sources of eBC-PM$_1$ were
199 evaluated for each factor utilizing a multilinear regression model, as suggested by Laborde et al., (2013); Zhu et al., (2018)
200 and Poulain et al., (2021), for instance. The following assumes that the eBC-PM$_1$ mass is associated with the separate
201 contribution from each OA factor (i.e., eBC-PM$_{1HOA}$, eBC-PM$_{1BBOA}$, and eBC-PM$_{1CCOA}$) at any time:

203 $$eBC(t) = eBC_{HOA}(t) + eBC_{BBOA}(t) + eBC_{CCOA}(t) \tag{3}$$

205 The eBC-PM$_1$ emission from each source is expected to be proportionate to the separate source mass concentration generated
206 in each season (m_{HOA}, m_{BBOA}, and m_{CCOA}, respectively). As a result, the multilinear regression model can be described as
207 follows:

209 $$eBC(t) = am_{HOA} + bm_{BBOA} + cm_{CCOA} \tag{4}$$

211 where a, b, and c are the linear regression coefficients for m_{HOA}, m_{BBOA}, and m_{CCOA}, respectively, that will be applied to evaluate
212 the contribution of eBC-PM$_1$ per each POA factor for each season (Table. S4).

2.6 Air mass trajectory analysis

214 Non-parametric wind regressions (NWR) were used to approximate the OA source concentrations at a given wind direction
215 and speed (Henry et al., 2009) in order to investigate not only the local but also the prevalent wind sector associated with
216 transported emission sources (Marin, et al., 2019). The NOAA HYbrid Single-Particle Lagrangian Integrated Trajectory
217 (HYSPLIT-4) model was used to analyse 96 h backward trajectories at 500 m above the model ground of the sampling place
218 (Draxler and Hess, 1997). The trajectory results were used for two independent but complementary analyses to better depict
219 the emission areas of the aerosol: by identifying the potential areas of aerosol sources and by clustering the trajectories.
220 A cluster analysis of the different trajectories was performed. The synoptic-scale air mass condition, together with geographical
221 locations and paths, is a crucial driver of local pollutant concentrations (e.g. Sun et al., 2020; Ma et al., 2014). Local particle
222 mass concentrations and meteorological conditions can play a significant role and be associated with specific air mass

223 trajectories. In addition, the trajectories of the air mass can influence aerosol compositions. For example, the stability of the
224 atmosphere is also meaningful since it influences both the vertical dilution of pollutants and the overall particle mass
225 concentrations. Therefore, the effects of inter-annual variations in air mass conditions and the stability of atmosphere on
226 observed patterns were inspected using a self-developed back-trajectory cluster method (BCLM), concerning air mass
227 backward trajectories, pseudo-potential temperature profiles, PM_{10} mass concentration profiles over Melpitz, and seasons
228 (Birmili et al., 2010; Ma et al., 2014).

229 In this method, the different clusters can be divided according to the different seasons (CS: cold season; TS: transition season;
230 and WS: warm season), and meteorological synoptic patterns (ST: stagnant; A1: anticyclonic with air mass coming from
231 Eastern Europe; A2: anticyclonic with air mass coming from the west; C1: cyclonic with air mass coming from relatively
232 south; C2: cyclonic with air mass coming from the west and south west). However, the clustering approach did not consider
233 spring and fall separately, and therefore the transition clusters correspond to both spring and fall. Finally, a total of fifteen
234 clusters were identified, corresponding to different meteorological conditions over the course of the year. Descriptive analysis,
235 cluster processing, and data processes and products are all described in detail by Sun et al., (2020) and Ma et al., (2014).

236 3 Results and discussion

237 3.1 PM$_1$ chemical composition

238 In this work, we investigate one-year-long measurements of PM_1 for Melpitz, Germany. All the data are presented in UTC,
239 during the winter and summer, the time zone is one and two hours behind local time, respectively. Yearly time series, seasonal
240 variation, and diurnal cycles of aerosol particle chemical compositions including mass concentrations and mass fractions, as
241 measured by ACSM and MAAP, are shown in Figures 1, 2, and 3, respectively. Over the entire period, the chemical
242 composition of PM_1 was basically made up of organic aerosol (46 % of the total mass; Fig. 1c), sulphate (16 %), nitrate (21
243 %), ammonium (11 %), eBC-PM_1 (6 %), and chloride (close to 0 %). However, a mean mass concentration of 10.49 µg/m^3
244 (Fig. 1) was obtained with an obvious seasonal trend which detected the highest total mass concentration (15.95 µg/m^3) during
245 the winter time and lowest mass concentration during the summer time; 6.24 µg/m^3 (Fig. 1a and Fig. 2a). Compared to previous
246 AMS measurements of Poulain et al., (2011) at the same station, a similar seasonal trend was observed in the period 2008/2009,
247 while the absolute masses differed (Table. S1), which is at least partially related to the inter-annual changes of the
248 meteorological conditions. Compared to previous ACSM long-term measurements of Poulain et al., (2021) at the same station,
249 a similar mean mass concentration of PM_1 was observed in the period from June 2012 to November 2017 (Poulain et al., 2021:
250 10.23 µg/m^3 and this study: 10.49 µg/m^3; respectively), and presented same seasonal trends for all the chemical species (Table.
251 S2) with a highest mass concentration in the winter and lowest mass concentration in the summer time (13.15 µg/m^3 and 7.64
252 µg/m^3, respectively; Table. S2). Consequently, the results obtained from the current study can be considered as a representative
253 ACSM study for Melpitz station. Fig. S3 presents the coming high polluted air masses for total PM_1 to the measurement site

254 in the current study; polluted Eastern Europe flow with high mass concentration and south-west with lower mass concentration
255 was more clearly found in winter time rather than in other seasons, which will be comprehensively discussed in the Sect. 3.4.
256 In comparison with other ACSM/AMS rural-background stations in Europe which can be divided into three parts Northern
257 Europe (NE), Southern Europe (SE), and Mid-latitude Europe (ME) (Bressi et al., 2021), the annual PM_1 mean mass
258 concentration measured at Melpitz is similar to the value obtained at other ME stations, such as Magadino 10.1 $\mu g/m^3$, Kosetice
259 8.5 $\mu g/m^3$ (Chen et al., 2022), 9.1 $\mu g/m^3$ on average of PM_1 mean mass concentration of 6 stations (Ispra, Melpitz, Magadino,
260 Cabauw, Sirta, and Hohenpeissenberg, Bressi et al., 2021).

261 **3.1.1 Inorganic**

262 The seasonality of the inorganic species can be associated with their variations in emissions and/or the changes in their
263 chemical atmospheric processes. Throughout the year, the mass concentration and their respective contribution to the total
264 PM_1 mass of nitrate, ammonium, and chloride increased from a minimum value in summer (11 %, 7 %, and 0 %, respectively;
265 Fig. 2b) and reached a maximum value in winter (24 %, 12 %, and 1 %, respectively; Fig. 2b). Moreover, the comparison
266 between Bressi et al., (2021) and current study (Fig. S4 from Bressi et al 2021, Fig. 3 from the current study) for Melpitz
267 station with different time coverage shows that the daily variation of ACSM sulphate, nitrate, and ammonium are similar in
268 both winter and summer seasons. In comparison with other ACSM/AMS rural-background stations in Europe (Fig. S4, Bressi
269 et al., 2021), the mean daily cycle of the PM_1 chemical components (sulphate, nitrate, and ammonium) does not show a similar
270 pattern to the other stations (Bressi et al., 2021) due to the different geographical location and meteorological conditions.
271 Sulphate showed a slightly different behavior. Although the contribution of sulphate to the total PM_1 decreased slightly from
272 summer (20 %) to winter (15 %), its mass concentration remained higher in winter compared to summer (2.38 $\mu g/m^3$ and 1.23
273 $\mu g/m^3$, respectively; Table. 1). The increment is not as drastic as other inorganic species since sulphate is least volatile,
274 therefore, more fraction of sulphate stayed in particle phase even in summer. Moreover, the sulphate contribution to the total
275 PM_1 was higher during the summer than winter time, since with enhanced irradiations in summer, sulphate formation from
276 photochemistry could be enhanced as well. This sulphate higher contribution in summer over winter is consistent with the
277 mean PM_1 mass concentration measured by AMS for the three periods during fall (16. September.2008 to 03. November.2008),
278 winter (24. February.2009 to 25. March.2009), and summer (23. May.2009 to 09. June.2009) campaigns reported by Poulain
279 et al., (2011). In comparison with previous ACSM long-term measurements of Poulain et al., (2021) at Melpitz station, a
280 similar mean mass concentration of sulphate was observed in the period from June 2012 to November 2017 (Poulain et al.,
281 2021: 1.54 $\mu g/m^3$ and this study: 1.67 $\mu g/m^3$; respectively; Table. S2). This comparison indicates the current study as a case
282 study of ACSM for Melpitz station within 5-year ACSM data, with the best data coverage of time in a year. The diurnal cycles
283 of sulphate (Fig. 3) showed a different daily pattern in warm and cold seasons. In summer, sulphate mass concentration
284 increased during the day and reached its maximum level at 12:00 UTC (Fig. 3) due to sulphur dioxide photochemical oxidation
285 processes in the atmosphere, which also presented the highest mass concentration during the day, along with maximum
286 temperature and sun radiation in summer time (Fig. S4). Furthermore, the NWR plots (Fig. S3) show that during the winter

9

time, sulphate mostly comes from the north and east sectors with wind speeds above 5 m/s which can be associated with dominant transported sulphate sources. Although the eastern wind sector remains visible for the sulphate in the summer time, the high concentrations of sulphate can be observed during periods with low wind speed and without a specific wind sector; which corresponds to local sulphate formation. Sect. 3.4 will go into detail about the long-range transported emissions later on. Although this locally formed emissions of sulphate (Fig. S3 and Fig. 9) can explain this peak during the day in summer, this photochemical process is not the only source of sulphate. It especially cannot explain the highest mass concentrations during the winter time with almost no diurnal variation (Fig. 3). For winter, the emission of domestic heating processes, which could be enhanced in the atmospheric boundary layer (Stieger et al., 2018), along with the long-range transported emissions, which came from north-east toward the measurement site (Fig. S3 and Fig. 9), and also high ammonium nitrate due to partitioning according to temperature, explain the high mass concentration but the low relative contribution of sulphate.

Nitrate is mostly found in the form of ammonium-nitrate (NH_4NO_3), which is reliant on the gas phase precursor concentrations, temperature, humidity, and aerosol chemical composition (Poulain et al. 2011; Stieger et al., 2018). Both nitrate and ammonium showed a minimum mass fraction and mass concentration in summer (11 %, 0.68 µg/m^3, 7 %, 0.43 µg/m^3, respectively; Fig. 2), an increasing trend toward the cold months and reached their maximum mass fraction and mass concentration in winter time (nitrate 24 %, 3.87 µg/m^3, ammonium 12 %, 2 µg/m^3, respectively; Fig. 2). The diurnal cycles of nitrate and ammonium (Fig. 3) showed a relatively similar daily pattern in all seasons, which means the highest values were reached in the morning, due to the beginning of vertical mixing and a reduction in the afternoon followed by an increase during the night, reflecting their night time production during every season. The volatile behaviour of ammonium-nitrate strongly affects its temporal variation during warm days leading to the formation of the gaseous nitric acid and ammonia compounds at higher temperatures and low humidity (Fig. S4, and S8). Nitrate profiles from NWR plots (Fig. S3) present two different wind directions for the whole period which might be associated with transported nitrate from Leipzig and Torgau (50 km in the south-west and 7 km in the north-east of Melpitz, respectively) with higher wind speed. Since the reaction pathway of OH and NO_2 can result in nitrate formation (Yang et al., 2022), this mechanism can be linked to traffic emissions in residential areas. These long-range transported sources together with locally formed emissions could describe higher mass concentrations for nitrate and ammonium due to e.g., meteorological conditions and abundant precursors in winter time. However, in winter, ammonium-nitrate remains mainly in the particle phase (Seinfeld and Pandis, 2006) since it can totally be changed from gas to particle phase at lower temperature (Spindler et al., 2010). High values of nitrate and ammonium in spring time are linked to agronomical fertilization (Stieger et al., 2018). These seasonal contribution results for both, nitrate and ammonium, are consistent with the previous AMS study (Poulain et al., 2011), with minimum fraction to the total AMS-PM$_1$ during summer (nitrate 5 % and ammonium 8 %; Table. S1), and maximum fraction during winter time (nitrate 34 % and ammonium 17 %; Table. S1). However, it is known that a fraction of the nitrate signal can be attributed to nitrogen containing organic species (Kiendler-Scharr et al., 2016), which can affect the overall nitrate mass concentration (Poulain et al., 2020).

321 Although chloride had the lowest annual mass concentration (0.05 µg/m^3) compared to all other PM$_1$ chemical components

322 (Table. 1), it showed the highest mass concentration and mass fraction in winter (0.11 µg/m^3, 1 %, respectively; Fig. 2a&b;

323 Table. 1) compared to other seasons; as seen in the previous AMS study of Poulain et al., (2011) (2 %, Table. S1). It could be

324 related to the surrounding and transported emissions which mass concentrations were high for air masses from north-easterly

325 and south-westerly directions (Fig. S3). In a multi-year analysis of the hourly PM$_{10}$ chloride mass concentration measurements

326 using a MARGA, Stieger et al., (2018) attributed the chloride sources of Melpitz during winter to the resuspension of road salt

327 used for the de-icing of streets, mainly coming from the cities of Torgau and Leipzig. These sites are also located in the wind

328 directions along with the coal and wood combustion emission region, which could explain the highest mass concentration of

329 chloride during the winter. Furthermore, the existence of chloride might be due to low mass concentration marine influences

330 consisting of sea-salt aerosols during all the seasons in the south-westerly direction (Fig. S3) which were previously studied

331 by Stieger et al., (2018). However, it is known that the AMS technology cannot properly detect sea salt (Huang et al., 2018;

332 Ovadnevaite et al., 2014) because the majority of chloride is in the refractory part which cannot be flash vaporized at 600 ºC.

333 Consequently, the chloride detected by the ACSM is mostly related to combustion processes (wood, coal combustion as well

334 as trash burning; Li et al., 2012).

3.1.2 eBC-PM$_1$ and organics

336 The eBC-PM$_1$ showed its maximum mass concentration and mass fraction to PM mass during winter time at 1.38 µg/m^3 and

337 9 %, respectively (Fig. 2), and only 0.25 µg/m^3 and 4 %, respectively, during summer time (Fig. 2). This is consistent with the

338 expected highest anthropogenic emissions from fossil fuel consumption (house heating and energy productions) in winter

339 compared to summer (Spindler et al., 2010). Furthermore, considering measured eBC-PM$_1$ in regard to wind speed and wind

340 direction from NWR plots (Fig. S3), eBC-PM$_1$ presented transported and local emissions. The highest mass concentrations for

341 fall, winter, and spring seasons could be linked to north-easterly and south-westerly winds with higher wind speed (above 10

342 m/s). While in summer time it is mostly linked to the surrounding emissions regardless of wind direction with lower wind

343 speed (Fig. S3). Significant changes in the diurnal profiles of eBC-PM$_1$ for the different seasons can be found with the highest

344 mass concentrations throughout the cold months compared to warm months owing to house heating (Fig. 3). It also showed

345 morning and evening peaks during all seasons (Fig. 3). This is consistent with those observed for the nitrogen oxides (Fig. S4),

346 which might be attributed to liquid fuel emissions and possibly the impact of the traffic rush hours on the main street, B 87,

347 located approximately 1 or 1.5 km north of the station, (Yuan et al., 2021). In the following chapter, diurnal patterns showed

348 lower mass concentrations at noon, and increased in the late afternoon to become nearly constant from 8 p.m. until midnight

349 (Fig. 3). This ambient particulate pollution resulting from very surrounding sources in the village was reported by van Pinxteren

350 et al., (2020). Diurnal increments of eBC-PM$_1$ were smaller in fall and spring compared to winter; the increment in summer is

351 also correspondingly low due to the absence of house heating emissions, and the diurnal variation in the increment is

352 determined by surrounding motor vehicle emissions in combination with the mixing layer height (van Pinxteren et al., 2020).

353 Further discussions on the seasonal trend of the eBC-PM$_1$ can be found in Sect. 3.3.

354

355 Organic aerosol (OA) was the predominant species throughout the whole year, with a mean mass concentration of 4.84 µg/m^3

356 and a mass fraction of 46 % (Fig. 1c; Table. 1). The OA mass fraction decreased from the maximum value in summer and

357 attained a minimum mass fraction in winter (58 %, 39 %, respectively; Fig. 2b). Similar to the comparison of previous inorganic

358 AMS measurements performed at Melpitz (Poulain et al., 2011), AMS-OA contribution to total PM$_1$ showed maximum

359 contribution during summer (59 %, Table. S1), and minimum contribution during winter (23 %) as well. However, the mass

360 concentration of OA increased from its lowest value in summer and reached its highest value in winter time (3.67 µg/m^3, 6.21

361 µg/m^3 respectively; Fig. 2, Table. 1). Similar to eBC-PM$_1$, by analyzing NWR plots, OA measured according to wind direction

362 and wind speed showed the highest average mass concentrations for north-easterly and south-westerly winds in winter (Fig.

363 S3). In fall, polluted air masses came from the north-easterly direction, and in spring and summer OA, surrounding emissions

364 closer to Melpitz were identified (Fig. S3). The diurnal cycle of the organic had an identical pattern across all seasons (Fig. 3),

365 showing the highest mass concentration in night time, a small peak in the early hours of the morning related to rush hours, and

366 the lowest mass concentrations around the early afternoon. The peak observed around 12:00 UTC in summer time (Fig.3) can

367 be due to the local photochemical production that leads to the formation of secondary organic aerosol mass during the day,

368 similar to the diurnal behavior of sulphate (previously discussed in Sect. 3.1.1). However, the reduction in total OA mass

369 concentration throughout the day (Fig. 3), which was mostly observed during the warm seasons (spring and summer), could

370 be clearly related to the dilution effect of increasing mixed layer height. During warm days, evaporation of semi-volatile

371 organics from the particle phase cannot be completely excluded (Schaap et al., 2004; Keck and Wittmaack, 2005). In

372 comparison between Bressi et al., (2021) and the current study for Melpitz station, the daily variation of organic are similar in

373 both winter and summer seasons, while there are differences between Melpitz with other rural-background stations due to the

374 different geographical location and meteorological conditions (Bressi et al., 2021).

375

376 Overall, eBC-PM$_1$ and OA can be composed of various sources with strong seasonal dependencies, as well as be influenced

377 by different responses to atmospheric dynamics depending on meteorological parameters, geographical locations, and chemical

378 processes. Therefore, a comprehensive analysis of the OA and eBC-PM$_1$ sources was performed using source apportionment

379 techniques.

380 **3.2 Source apportionment of OA**

381 The chosen solution for the organic aerosol source apportionment contained five different factors based on their time series

382 and mass spectra (Fig. 4). The source apportionment solution is based on a partly constrained rolling approach with three

383 primary organic factors (POA), namely HOA (on average 0.30 µg/m^3 and 6 % of the total OA; Table.1 and Fig. 4), BBOA (on

384 average 0.39 µg/m^3 and 7.9 % of the total OA) and CCOA (on average 0.77 µg/m^3 and 15.4 % of the total OA). In addition to

385 these POA factors, two oxygenated organic aerosols (OOAs) were identified as LO-OOA (on average 1.62 µg/m^3 and 32.4 %

386 of the total OA), and MO-OOA (on average 1.92 µg/m^3 and 38.4 % of the OA). The seasonal average mass concentrations and

387 relative mass fractions of each OA factor to the total OA mass and their seasonal diurnal variation are presented in Figures 5

388 and 6; respectively. They will be discussed separately in the following sections.

3.2.1 POA factors

390 The HOA mass spectrum (Fig. 4b) is recognized by mass fragments at unsaturated and saturated hydrocarbon chain pairs *m/z*

391 41 (C_3H_5), 43 (C_3H_7), *m/z* 55 (C_4H_7) and 57 (C_4H_9) (Zhang et al., 2005; Canagaratna et al., 2004), which are representative of

392 liquid fuel combustion emissions and are associated with either traffic emissions or domestic heating fuel (Wang et al., 2020).

393 This result designates HOA as a minimal source of OA at the monitoring site, which is consistent with previous studies in the

394 PM_1 range made in the same place: a) total average was 7 % of the organic mass concentration in a study by Crippa et al.,

395 (2014) total average was 3 % of PM size range between 0.05-1.2 µm mass concentration in a study by van Pinxteren et al.,

396 (2016) (Table. S3). However, in comparison with other ACSM/AMS stations in Europe (22 stations; Chen et al., 2022),

397 Kosetice with 9.7 % as a rural-background site, and Bucharest with 13.7 % as an urban-background site showed the minimum

398 annual HOA mean contribution of total OA, which is similar to the contribution at Melpitz.

399 Mass concentration of HOA followed a slightly increasing seasonal pattern towards the cold months, from 0.23 µg/m^3 in

400 summer to 0.36 µg/m^3 in the winter (Fig. 5a; Table. 1). HOA presented a low correlation with nitrogen oxides over the entire

401 period (R^2= 0.17, Table. 1), but it correlated well with eBC-PM_1 in winter (R^2= 0.52; Table. 1) and showed a weaker correlation

402 in summer (R^2= 0.28; Table. 1). Possibly HOA is also associated with household heating (35 % by oil and 11 % by liquid

403 petroleum gas, van Pinxteren et al., 2020) rather than traffic emissions, especially during the cold months. Analyzing the NWR

404 plots demonstrates the highest HOA mass concentration was observed at low wind speed during the warm period (Fig. 7)

405 indicating, rather local emission sources. While during the cold period a clear increase of the mass concentration can be

406 associated with the highest wind speed (> 10 m/s) mostly coming from the North to East sector. During periods with wind

407 speeds below 10 m/s, the two dominant wind sectors (NE and SW) can be observed. The first one might be associated with

408 emission plumes coming from either the surrounding traffic emissions (the federal street B 87), as well as the domestic

409 emissions are associated not with house heating in summer but with hot water production (van Pinxteren et al., 2020), as well

410 as the city of Torgau (with approx. 20,000 inhabitants, distance from 7 km). Although the SW sector shows a lower HOA mass

411 concentration in comparison to the NE one, it corresponds to the direction of the city of Leipzig (above 600 000 inhabitants,

412 approx. 50 km). Therefore, it might be associated with the influence of the pollution plume of the city of Leipzig.

413 The diurnal patterns of HOA reproduced two peaks in the morning and evening for all seasons (Fig. 6), which is related to

414 traffic rush hours and linked to surrounding emissions from the main street (B 87, approx. 1.5 km north of the station), Melpitz

415 village itself, and emissions coming from Leipzig and Torgau residential areas. The small time shift for the start of the evening

416 increase corresponds to the time shift of the sunrise between winter and summer. The diurnal cycles reached a systematic

417 minimum during the day time probably not only owing to emission decrease but also emphasizing the effect of dynamic

418 atmospheric processes (e.g. mixing layer height (MLH) and planetary boundary layer (PBL)) (Fig. 6, and S4). Oppositely to

419 what can be seen during the day time, night time mass concentrations appeared to be unaffected by the seasons, showing

13

similar mass concentrations all year round, i.e. their mass concentration rose continuously in the early evening and remained at a very similar mass concentration over the night, which supports the hypothesis of yearlong continuous rather surrounding emissions. Nevertheless, the differences between HOA mass concentration during the night time from summer to winter season (Fig. 6) are small and can be covered by the uncertainties of PMF result ($\pm$ 32.5 %, Fig. S2), however, it can be explained by different emission sources, condensation of POA (Chen et al., 2022), evaporation, oxidation processes (Saha, et al., 2018), and potential night time aging process by high ozone concentration (Kodros, et al., 2020).

The mass spectra of BBOA are identified by ions at m/z 29, 43, 60, and 73 (Fig. 4b), known as fragments tracers of anhydro-sugars like levoglucosan (Alfarra et al., 2007), which have been recognized as indicators of wood combustion processes (Simoneit et al., 1999; Simoneit and Elias, 2001). This is confirmed by the correlation between BBOA and levoglucosan over the whole period (R^2= 0.65; Table. 1). On average, BBOA mass concentration and contribution were 0.39 µg/m^3 and 7.9 %, respectively (Table. 1 and Fig. 4a). However, its contribution is highest during winter time (10.6 %; Fig. 5), which is similar to previous studies in different PM ranges for the Melpitz station during the cold months: a) in PM$_1$ range, 14 % of OA mass concentration in fall (Crippa et al., 2014); b) in 0.05-1.2 µm range, highest contribution with 10 % of PM mass concentration in winter (van Pinxteren et al., 2016); and c) in PM$_{10}$ range, highest contribution with 16 % of PM mass concentration in winter (van Pinxteren et al., 2020).

By analyzing the NWR model, the high mass concentration of BBOA in cold months, regardless of wind speed can be observed with two wind sectors coming from north-east and south-west directions. These BBOA emissions are mainly attributed to residential heating in Melpitz village and also indicate the effect of transported biomass burning emissions to the sampling site with higher wind speed (> 10 m/s, Fig. 7). While in summer time, it is still observable as surrounding emissions during periods of low wind speed (Fig. 7 and Fig. S4) with a mass concentration of 0.21 µg/m^3 and a contribution of 6.1 % to total OA (Fig. 5). The presence of BBOA in the summer can be linked to water heating systems using wood briquettes and logs (estimated at 32 % of total central heating in this area, van Pinxteren et al., 2020). Moreover, it can also be related to recreational open fires and/or barbecue activities (van Pinxteren et al., 2020). This result is similar to other ACSM/AMS rural-background stations in Europe (22 stations; Chen et al., 2022); both Magadino and Kosetice showed the highest contribution of BBOA during winter time (27.4 % and 15.5 % respectively).

The diurnal cycles, peaking from early evening to early morning in winter (Fig. 6), match the expectations for a factor related to domestic heating activities, along with a better eBC-PM$_1$ correlation during winter than during summer time (R^2= 0.81, and R^2= 0.42, respectively; Table. 1). Finally, in opposition to HOA, the night time BBOA mass concentration showed a strong seasonal variation, having its highest mass concentration during winter nights and lowest during summer time, the influence of the impact of house heating emissions on the BBOA emissions. However, the day time behavior reflects the influence of enhanced vertical mixing during day time (higher temperature, Fig. S4) combined with high wind speeds can readily cause dilution and thus low pollutant concentrations near the ground (Chen et al., 2021; Via et al., 2020; Paglione et al., 2020).

454 The mass spectrum of CCOA is characterized by fragments at m/z 77, 91, and 115 (Fig. 4b) as previously reported by Dall'Osto

455 et al., (2013); Xu et al., (2020); Tobler et al., (2021) and Chen et al., (2022). These specific fragments can be associated with

456 unsaturated hydrocarbons, particularly ion peaks related to polycyclic aromatic hydrocarbon (PAH). The CCOA time series

457 showed the strongest correlation with eBC-PM$_1$ (R^2= 0.9; Table. 1). In addition, several studies reported that coal combustion

458 emissions are often accompanied by high chloride mass concentrations (e.g; Iapalucci et al., 1969; Yudovich and Ketris, 2006

459 and Tobler et al., 2021). Here, the correlation between CCOA and chloride was higher during winter than during summer time

460 (R^2= 0.41, 0.15 respectively; Table. 1), as the gas-particle phase equilibrium dramatically changes with rising temperatures

461 (Tobler et al., 2021). Although chloride is almost observable in the particle phase as ammonium chloride (NH_4Cl) at lower

462 temperatures, chloride is typically observable in the gas phase as hydrogen chloride (HCl) at higher temperatures (Tobler et

463 al., 2021).

464 CCOA represented on average 15.4 % of the total OA (0.77 µg m^{-3}), (Table. 1; Fig. 4a) and is the most important POA over

465 the entire period. No CCOA factor was identified in the previous AMS measurements made at Melpitz (Crippa et al., 2014).

466 Most likely this factor was not properly resolved and/or it was not possible to properly separate it from the other factors since

467 no reference mass spectra for CCOA were reported in the literature at that time. CCOA showed the highest mass concentration

468 and mass fraction during the winter (1.58 µg/m^3, 23 %, respectively; Fig. 5a; Table. 1). By analyzing the NWR plots, this high

469 mass concentration during winter time can be related to the surrounding emissions and long-range transported air masses

470 coming from two different directions, north-easterly and south-westerly (Fig. 7). Not surprisingly, the lowest mass

471 concentration and contribution were observed during the summer time (0.30 µg/m^3, 8.7 %, respectively; Fig. 5a; Table. 1,)

472 which most probably correspond to only long-range transport as later discussed in Sect. 3.4 (Fig. 9). Moreover, this result is

473 consistent with previous measurements made in the same place. For the size range 0.05-1.2 µm van Pinxteren et al., (2016)

474 reported a contribution of 29 % and 21 % of the PM in winter and summer respectively, and a contribution of 7 % and 0 % for

475 winter and summer respectively for the PM$_{10}$ range was found (van Pinxteren et al., 2020). From all ACSM/AMS stations (22

476 stations; Chen et al., 2022) only Melpitz as a rural-background site and Krakow as an urban-background site showed the coal

477 combustion emissions with the maximum contribution during winter for both sites (Krakow: 18.2 % and Melpitz: 23 %)

478 compared to summer (Krakow: 4.5 % and Melpitz: 8.7%). The drastic seasonal changes in Krakow are attributed to the

479 common use of coal burning for residential heating reasons during the winter time (Tobler et al., 2021), while in Melpitz, as

480 discussed above, coal combustion is affected by both surrounding and transported emissions from other sites. Mass

481 concentrations of CCOA during night time were much higher than during day time throughout all seasons (Fig. 6), further

482 verifying the increased coal combustion emissions from coal heat generation at night in winter time and the potential decrease

483 in emissions during the day due to a strong influence of atmospheric dynamics.

484 **3.2.2 OOA factors**

485 The two OOAs (Fig. 4) referred to as LO-OOA and MO-OOA are known to be characterized by the different ratios of their

486 m/z 43 and m/z 44 fragments (Fig. 4b), which represent the oxidation level (Canagaratna et al., 2015). While m/z 43 could be

derived from $C_2H_3O^+$ (a signature of the semi-volatile) and/or $C_3H_7^+$ (a signature of the primary emissions of the hydrocarbon-like), m/z 44 is mainly derived from the fragment of CO_2^+ (a signature of oxygenated, particularly acids) (Canonaco et al., 2015; Ng et al., 2010). As presented in Fig. 4b, MO-OOA mass spectra showed a notable peak at m/z 44. This spectrum has been extensively recognized as low volatility OOA (LV-OOA) and described to be made-up of aged secondary OA (SOA) and highly oxidized OA (Ulbrich et al., 2009; Zhang et al., 2011; Ng et al., 2011); while the mass spectra of LO-OOA in this study presented a higher m/z 43 (Figs. 4b) compared to MO-OOA, which is similar to the mass spectral pattern of the previously reported freshly formed semi-volatile OOA (SV-OOA) (Jimenez et al., 2009; Ng et al., 2010). To differentiate the variations of the OOAs factor, the $f44$ vs $f43$ space was used which is a typical diagnostic tool based on atmospheric aging (Ng et al., 2010).

The seasonal $f44/ f43$ for OOAs measured points and the $f44/ f43$ for modelled factor profiles (LO-OOA and MO-OOA) are presented in Fig. S5. The data points in Fig. S5 are distributed differently according to the season (Chen et al., 2021; Canonaco et al., 2015; Crippa et al., 2014; Chazeau et al., 2022). Furthermore, the modelled factor profile points represent a high variability in space, especially for LO-OOA. This assumes how an annual or seasonal PMF solution, unless a larger number of factors are used, would perform poorly in capturing all of the variations of SOA. In order to capture time-dependent changes, in particular for LO-OOA, it is, therefore, advantageous to perform rolling PMF analysis. The triangle plot defined by Ng et al. (2010) is also shown in Fig. S5. As assumed the LO-OOA points were concentrated in the lower part of the space, whereas more aged MO-OOA points relocated to the upper part of the space during the aging process. The fall, spring, and summer data points were all located on the right side of the triangle (Fig. S5), however, the winter data points were located near the top and inside the triangle. The data points on the right side of the triangle correspond to the time exposed to higher temperatures more than those that are within the triangle. This could be attributed to an increase in biogenic SOA emissions if the temperature increased, as biogenic OOA appears to be dispersed all along the right side of the triangle. Furthermore, as the temperature is reduced, the increased biomass emissions cause the OOA points to lie vertically inside the triangle, as seen in the winter data.

The two OOAs were the two most significant contributors to the total OA fraction (Fig. 4) over the entire period. The seasonal mean mass concentrations of MO-OOA varied from higher mass concentrations during winter (2.25 µg/m^3) and lower during summer time (1.44 µg/m^3, Table. 1). However, the highest MO-OOA mass concentrations found during the cold periods are similar to the seasonal patterns in POA. This high mass concentration in cold seasons can be seen from the NWR plot (Fig. 7) presenting local emissions with low wind speed (> 5 m/s) and transported emissions from east, north-east, and south-west directions with high wind speed (< 5 m/s). Furthermore, high mass concentrations of MO-OOA are generally found at high relative humidity (RH > 80 %) and low temperature (< 0 °C), i.e., conditions during winter time (Fig. S6). This low air temperature condition can be linked to a possible scenario for an increase in the MO-OOA precursor emissions from biomass burning and coal combustion as a result of residential heating activities during winter time. Therefore, significant enhancement appears to be an effect of RH during winter, proposing that the aqueous-phase heterogeneous mechanisms could also play a

16

crucial way in the regional MO-OOA formation through winter as suggested by Gilardoni et al., (2016). In contrast, no RH-temperature-dependent trends for the MO-OOA were found in the other seasons (Fig. S6), indicating more complex formation processes during other seasons. Meanwhile, MO-OOA diurnal cycles presented a seasonal variation as well, with a remarkable enhancement in the evening and night time during winter (Fig. 6), indicating a potential regional formation mechanism containing night time chemistry (Tiitta et al., 2016), and descending pattern from night time to day time due to planetary boundary layer effect. While in fall, spring, and summer, MO-OOA displayed a considerable increase during the day (Fig. 6), indicating that higher temperatures result in considerable regional photochemical production of SOA particles (Fig. S4) and enhanced solar radiation (Petit et al., 2015). Furthermore, regarding the correlation of mass concentration of MO-OOA with sulphate, the latter is regarded as a local secondary production indicator (Petit et al., 2015, and Table. 1). Consequently, alongside almost stable mass spectra throughout the year, MO-OOA seems to be derived from a variety of seasonal-dependent formation mechanisms and sources (such as aged background, biomass burning, coal combustion, and biogenic sources).

The seasonal mean mass concentrations of LO-OOA varied from higher mass concentrations during fall (2.13 µg/m^3) and lower mass concentrations during spring time (1.24 µg/m^3, Table. 1). Temperature had a significant effect on LO-OOA, and showed a distinguishable seasonal variation pattern. The temperature-RH dependence of the LO-OOA was not quite similar depending on the season (Fig. S6). The highest winter time LO-OOA mass concentrations were found mostly at low temperatures and high RH environments, indicating that gas-particle partitioning might have a key role in LO-OOA formation throughout this season. The freshly formed SOA deriving from primary biomass burning and coal combustion emissions, as found in previous studies (Crippa et al., 2013; Zhang et al., 2015; Y. Sun et al., 2018; Stavroulas et al., 2019) can also affect the LO-OOA during the cold months. Furthermore, since nitrate could be originated locally or arrived from a long distance to Melpitz (Sect. 3.1.1), with a good correlation between LO-OOA and nitrate ($R^2= 0.59$) during winter, the long-range transported LO-OOA from different directions reaching to measuring site could be explained (Fig. 7). Different LO-OOA daily cycles were also found in different seasons (Fig. 6). The daily changes in LO-OOA displayed higher mass concentrations in night time compared to day time in fall, spring, and summer (Fig. 6), highlighting the significant roles of night time chemistry and/or gas-particle partitioning in the LO-OOA formation; while the decrease during the day is partly linked to the atmospheric dilution effect (Fig. S4), evaporation and photochemical aging into MO-OOA (Fig. 6). For winter night increments, lower temperature in favor of condensation; and more abundant precursors present considering increased BBOA emission, therefore enhanced night-chemistry activities, leads to higher LO-OOA; moreover, shallow boundary layer in winter and night time inversion caused pollutants to accumulate.

3.3 Source apportionment of eBC-PM$_1$

By applying a multilinear regression model, during the source apportionment analysis, eBC-PM$_1$ correlated with every one of the three identified primary organic factors (HOA, BBOA, and CCOA, Table. 1). CCOA appeared to be the largest source of eBC-PM$_1$, contributing half of it (eBC-PM$_1$-CCOA 55 %, Table. 1), followed by eBC-PM$_1$ associated with BBOA 37 % (eBC-

554 PM$_1$-BBOA), while the lowest contribution was found for eBC-PM$_1$-HOA (8 %). However, the contribution of sources to the

555 total eBC-PM$_1$ strongly depends on the season. Looking at each individual source, the hydrocarbon-like emissions contributed

556 most to the eBC-PM$_1$ fraction in the fall (eBC-PM$_1$-HOA with 22 %, Table. 1; Fig. 8b), while biomass burning emissions

557 dominated the eBC-PM$_1$ in summer and coal combustion emission dominated in winter (eBC-PM$_1$-BBOA and eBC-PM$_1$-

558 CCOA with 69 % and 56 %, Table. 1). In the diurnal cycle, contribution to the total eBC-PM$_1$ of eBC-PM$_1$-HOA showed two

559 peaks in the morning and evening for fall, spring, and summer (Fig. S7), reflecting the impact of the traffic rush hours as

560 mentioned in Sect. 3.2.1, and the minimum contributions during the day time due to the effect of lowest emissions and PBL

561 effect (Fig. S4). However, winter time did not show a strong variation in the diurnal cycle (Fig. S7). This indicates the potential

562 influence of continuous emissions at the measurement site. Biomass burning combustion with its maximum contribution during

563 the day in summer (Fig. S7) can be related to a variety of different eBC-PM$_1$-POA mass concentrations (Fig. S7b), while the

564 BBOA mass concentration was almost constant, the other POA mass concentration decreased during the day. Coal combustion

565 showed an increasing contribution during night time in all the seasons (Fig. S7), especially during the winter time, which

566 further confirms the enhanced coal combustion emission in winter nights (Fig. S7b).

3.4 Seasonal air mass clustering

568 As mentioned before, the geographical origin of the PM$_1$ chemical species and also PMF components are not only emitted

569 from the surrounding area but also transported. Therefore, to better identify the origin of their sources, trajectory analysis, and

570 their clustering analysis were applied using the self-developed back-trajectory cluster method (BCLM) (Sun et al., 2020; Ma

571 et al., 2014; Hussein et al., 2006). Regarding this cluster approach, six air masses were identified at Melpitz station for the

572 winter season, four air masses for the transition seasons, and five air masses for the summer season (Fig. 9a). The number of

573 clusters with their corresponding mean mass concentration of PM$_1$ chemical species and PMF factors of organics are

574 summarized in Table. 2 and with more details in Tables S4 and S5.

3.4.1 Winter

576 Fig. 9b and 9c illustrate the mass concentration and contribution of PM$_1$ chemical species and PMF factors of organic for each

577 air mass type at Melpitz based on the type of air masses. For the winter season, the cluster CS-ST corresponds to more

578 surrounding emission origin with a PM mean value of 21.95 µg/m^3, which occurred during 14 % of the total measurement

579 period. These surrounding emissions refer to the emissions from Melpitz station directly, Melpitz village, and short distance

580 transported particles like particles from Leipzig and Torgau. This cluster presented the highest mass concentration of LO-OOA

581 to the PM mass (2.73 µg/m^3). In fact, SOA is considered to be formed by biomass burning as well as coal combustion,

582 particularly during the winter when biogenic emissions and UV radiation are low (Lanz et al., 2010; Kodros, et al., 2020). In

583 this condition and in the presence of NO$_2$ and O$_3$, the biomass burning emissions could age rapidly and produce SOA. In

584 conclusion, this cluster could confirm the role of freshly formed SOA which originated from the primary biomass burning and

585 coal combustion emission (mass concentrations of 0.97 µg/m^3 and 1.89 µg/m^3, respectively). Furthermore, nitrate showed a

18

586 high mass concentration and contribution in this air mass (5.38 µg/m^3 and 25 %, respectively) due to e.g., meteorological

587 conditions and abundant precursors.

588 The cluster CS-A1 with the highest mass concentration of PM (29.14 µg/m^3) represented Eastern European continental air

589 masses (passing Poland and the Czech Republic) during anticyclonic flow which occurred during 18 % of the total

590 measurement period, meaning that Melpitz was under their influence during winter. This air mass, with the highest POA mass

591 concentration (5.56 µg/m^3), especially coal combustion emissions (CCOA and eBC-PM$_1$-CCOA with an average mass

592 concentration of 4.01 µg/m^3 and 1.93 µg/m^3, respectively), highlight the importance of long-range transported emissions. This

593 cluster also contained the highest mass concentration of sulphate (5.39 µg/m^3) and could support the importance of coal

594 combustion on sulphate formation, which is known to be strongly emitted by coal power plants (Wierońska-Wiśniewska et al.,

595 2022).

596 The air mass CS-A2 identified as marine-influenced air mass with a mean value of 13.39 µg/m^3 of PM came from the United

597 Kingdom with the anticyclonic flow, which occurred during 8 % of the total measurement period. This cluster presented a low

598 mass concentration of POA and for two OOAs almost the same mass concentration and contribution (Table. S5 and Table.

599 S6). Since Melpitz is placed away from the coast, therefore the sampling location is affected by aged maritime air masses

600 (Poulain et al., 2011). Inorganics are dominated by nitrate in this cluster with the high mass concentration (3. 86 µg/m^3) which

601 represents the highest mass fraction (50 % of the total inorganic species).

602 The CS-C1 air mass with a mean value of 15.99 µg/m^3 characteristic of Southern European air mass, came from an industrial

603 and polluted area starting from Spain and partly crossing Italy with the cyclonic flow, which occurred during 10 % of the total

604 measurement period. POA mass concentration and contribution were low in this cluster, while SOA, especially MO-OOA,

605 showed the highest mass concentration of PM over the entire period (3.77 µg/m^3) and the highest contribution during the winter

606 season (24 %). This can be linked to the high sulphate in this air mass (2.99 µg/m^3), which showed that the regional influence

607 by contribution from aged BBOA and CCOA might be manifested in MO-OOA (as discussed in Sect. 3.2.2).

608 Finally, CS-C2a and CS-C2b were both associated with cyclonic and marine influence conditions which only occurred for a

609 short time (3 % and 2 % of the total measurements, respectively), showing the lowest PM mean value (4.09 µg/m^3 and 2.60

610 µg/m^3, respectively). Both of them showed almost the same mass concentration and contribution of POA (Fig. 8a and b; and

611 Table. S5 and S6). However, similar to CS-A2, cluster CS-C2a contained a marine component at the beginning point of the

612 air masses, and in the following time it was dominated by continental areas (France and southern Germany), where due to the

613 longer time transferring over continent and aging process, it showed more nitrate mass concentration and contribution than

614 CS-C2b (1.35 µg/m^3, 16 µg/m^3; and 28 % 14 %, respectively). Whereas CS-C2b started near Iceland with same history of the

615 air mass over the continent, and in comparison, with CS-C2a, it presented a higher contribution of sulphate (29 % and 19 %,

616 respectively), which could be associated with aged marine air mass due to the higher contribution of MO-OOA (21 % and 18

617 %, respectively).

3.4.2 Transition seasons

For transition seasons (fall and spring), whereas the four clusters showed quite similar PM mass concentrations (Fig. 9) which might be linked to the overall weather situation during these two times of the year, their chemical composition strongly depended on their origins. TS-A1 and TS-A2 corresponded to two different types of anticyclonic air masses with respective mean PM mass concentrations of 6.06 µg/m^3 and 5.86 µg/m^3. Cluster TS-A1 which occurred during 4 % of the total measurements period, started from Finland, crossing the Estonian, Latvian, Lithuanian, and Polish coasts before arriving at Melpitz. Although it might contain a certain marine component, this cluster mostly followed coastal areas, which means that in this cluster OA mass concentration dominated PM (2.95 µg/m^3). Furthermore, this cluster showed continental and polluted aspects with the highest LO-OOA mass concentration and contribution during transition seasons (1.03 µg/m^3 and 17 % respectively), which is linked to originating from freshly formed SOA from primary biomass burning and coal combustion emissions around coastal areas. On the other hand, cluster TS-A2 (4 % of the measurement period) is characterized as a marine cluster and started from the south of Iceland/Greenland. This cluster showed inorganics as the dominant components in PM with a high mass concentration and a mass fraction (3.35 µg/m^3 and 58 % respectively). Since Melpitz is influenced by aged marine air masses, this cluster showed a maximum nitrate mass concentration during the transition seasons (1.54 µg/m^3 and a contribution of 26 %, respectively).

Finally, two other clusters TS-C1 and TS-C2 were two different types of cyclonic air masses in fall and spring time, with mean PM mass concentrations of 4.69 µg/m^3 and 4.94 µg/m^3 respectively. These trajectories with different types of marine influenced air masses occurred for a very short period of time (3 % and 4 % of the total measurements period, respectively). The first one, TS-C1, started from the Atlantic Ocean near Spain and is associated with a more continental influence, which is why organic mass concentration and contribution were higher than inorganics. However, The LO-OOA contribution of this cluster was the highest during this time period (26 %) due to the aging processes of primary organic aerosols especially CCOA, which had a maximum mass concentration (0.31 µg/m^3 and mass fraction of 7 %, respectively). While the second one, TS-C2, was almost a pure marine cluster, coming from the Norwegian Sea. In opposition to TS-C1, PM was dominated by inorganics in TS-C2, with a high mass concentration of nitrate (1.35 µg/m^3) representing the aging effect due to the long-time transfer over the continents.

3.4.3 Summer

During the summer season, the different clusters showed strong changes in both chemical compositions and total mass concentrations. Cluster WS-ST was identified as the local air mass with a mean value of 8.97 µg/m^3, which occurred for a short period, 6 % of the measurement. However, this cluster contained a low POA mass concentration but a maximum contribution of MO-OOA (32 %), assuming important regional photochemical roles of SOA particles with higher temperatures (Fig. S4) and enhanced solar radiation (Petit et al., 2015).

649 Air masses WS-A1 and WS-A2 were two different types of anticyclonic air masses with different directions and different
650 mean PM mass concentrations. Cluster WS-A1, known as the highest mass concentration during summer time, (16.95 µg/m^3
651 and contribution of 11 % of the measurement period) was the continental air mass which was coming from Eastern Europe
652 during the anticyclonic flow (starting from Belarus, crossing Poland and the Czech Republic). This air mass included maximum
653 inorganics and organics especially CCOA mass concentration (1.28 µg/m^3) during summer time, which can explain the existing
654 higher CCOA during summer, and showed the role of long-range transported emissions in the summer season. However, WS-
655 A2 air mass, with a mean value of 9.48 µg/m^3 was a marine-influenced air masse and was coming from the North Sea, which
656 only occurred for a short period (6 % of the total measurement period).

657 Moreover, two cyclonic air masses, WS-C1 and WS-C2, were also identified as two different marine clusters. These trajectories
658 did not occur very often, only 5 % and 3 % of the total measurement period, respectively. The starting point of WS-C1 with a
659 mean value of 8.41 µg/m^3 was the Celtic Sea, but in the following time, it predominantly passed over continental areas (France
660 and southern Germany), which means it could be aged and the result can be shown in the high mass concentration of nitrate
661 and sulphate in this cluster (1.63 µg/m^3 and 1.86 µg/m^3, respectively). Finally, the starting point of WS-C2 with a mean value
662 of 4.46 µg/m3, was near Iceland, with the lowest PM mass concentration during summer. However, it showed the highest
663 sulphate contribution (27 %) at this time which could be associated with aged marine air mass like other marine air masses.

3.4.4 Cluster seasonality

665 A parallel comparison can be made between the winter and summer clusters. Clusters CS-A1 and WS-A1 both show the
666 highest POA contribution dominated by coal combustion, which emphasizes that the origin of this source could be associated
667 with the transport of the coal power plants emissions from Eastern Europe (e.g. Eastern part of Germany, Poland, Czech
668 Republic and further countries located in the East). These clusters were not only affected by the winter air quality but also the
669 summer air quality.

670 Clusters CS-ST and WS-ST, which were known as local air masses, showed the seasonal effect on the chemical component.
671 First, the volatility of ammonium nitrate at higher summer temperatures could explain their lower value in summer. Then,
672 atmospheric photochemical oxidation processes affected the sulphate locally formed emission in summer, which its highest
673 value over inorganic components during summer can be confirmed. Not surprisingly, due to the residential heating effect, POA
674 mass concentration was very high during winter; however, freshly formed SOA originating from biomass and coal emissions
675 can explain the higher LO-OOA mass concentration in winter.

676 During the whole period, some marine air masses with cyclonic and anticyclonic flow showed the important roles of aged
677 marine air masses over the measurement site: a) clusters CS-A2 and WS-A2 with anticyclonic pattern starting from the North
678 and/or Norwegian Sea, and b) CS-C2a, WS-C1, and TS-C1 starting from the Celtic Sea near Spain, and also CS-C2b and WS-
679 C2 starting from Iceland, all with cyclonic patterns contain nitrate and sulphate during the transferring over the continental
680 areas in different seasons.

4 Conclusion

The chemical compositions of non-refractory fine aerosol (NR-PM$_1$) at the German rural-background observatory Melpitz were investigated in this study over a one-year period between September 2016 and August 2017. Overall, the averaged total PM$_1$ mass concentration is 10.49 μg/m^3 and follows a clear seasonal pattern, with the highest mass concentration during winter (15.95 μg/m^3) and the lowest mass concentration during summer time (6.24 μg/m^3). The organic aerosol was the most significant component, accounting for 46% of total PM$_1$ and showing significant seasonal dependency (39 % in winter to 58 % in summer). It was followed by sulphate (15 % and 20 %) and nitrate (24 % and 11 %). For OA source apportionment, PMF in a rolling fashion has been applied using the SoFi Pro, which provided the decomposition of time-dependent factor profiles that were able to better capture the variability of OA sources across seasons in comparison with the conventional seasonal PMF. The final solution enabled the identification of five factors throughout the one-year measurements of OA; HOA, BBOA, CCOA, LO-OOA, and MO-OOA. Using the correlation between HOA, BBOA, and CCOA with eBC-PM$_1$, a multilinear regression approach was applied to perform the source apportionment of eBC-PM$_1$.

Generally, in Melpitz, HOA as a minor source of OA (6 % of the contribution of total organic mass) and eBC-PM$_1$ (8 % of the total eBC-PM$_1$) was associated with: a) low traffic emissions, b) household heating in winter, and c) the central heating for hot water production for all the seasons which uses multiple fuel types in the Melpitz area. BBOA representing 7.9 % of the contribution of total organic mass and 37 % of the total eBC-PM$_1$, showed a seasonal effect, emphasizing the impact of house heating during winter. Similar to HOA, the presence of BBOA during summer was due to central heating which uses multiple fuel types in the Melpitz area. The most dominant anthropogenic source was associated with CCOA with a 15.4 % contribution of total organic mass and 55 % of the total eBC-PM$_1$ with the highest mass concentration and contribution of PM during winter rather than summer. Although a certain fraction of CCOA could be linked to surrounding domestic heating (van Pinxteren et al., 2020), it is rather associated with power plant emissions and long-range transport all year round which is supported by cluster and back-trajectory analysis. LO-OOA and MO-OOA referred to oxidized oxygenated organic aerosol (32.4 % and 38.4 % of the contribution of total organic mass, respectively), were identified as a secondary organic aerosol with the highest mass concentration during the cold months and the lowest mass concentration during the warm months. LO-OOA mass concentration decreased during the day due to dilution, and the evaporation process resulted in aging into MO-OOA.

A combination of the NWR model and cluster analysis was used to better understand the origin of the aerosol reaching the station. Overall, Melpitz is influenced by fifteen types of air masses, such as long-range continental, marine, and surrounding emissions. During winter and summer time, easterly continental air masses, CS-A1 and WS-A1 with an anticyclonic pattern come from Eastern Europe and showed a significant particle mass concentration, especially high POA (and CCOA) mass concentration at the measurement site. Marine clusters, mostly coming from the south/west/north side with aged marine air masses including nitrate and sulphate, also have important roles in the PM mass concentration at the Melpitz site over the entire period (winter: CS-A2, CS-C2b, and CS-C2a, transition: TS-C, TS-A2 and TS-C2, and summer: WS-Ca, WS-C2, and

WS-A2). However, the surrounding emissions are recognized as another important source of emissions which include high organic and inorganic components during winter and summer (CS-ST and WS-ST, respectively).

Our results emphasize the importance of the long-range transported emissions of coal combustion related aerosol particles regardless of the season, which supports that the main CCOA source is related to coal power plants emissions. However, coal power plants emissions not only affect the surrounding air quality but can also be transported over long distances. It is important to note that the overall coal combustion mass concentration presented here can certainly be underestimated since the identified CCOA factor is associated with freshly emitted organic aerosol and no factor associated with potential aged coal combustion was identified. Because coal still is an important energy source in the European energy mix (68.4 % of all energy in the EU was produced from coal, crude oil, and natural gas, Energy Statistics - an Overview - Statistics Explained, 2022) as well as on a global scale and also that it still will be in use for the coming decades (until 2040, Europe's Coal Exit - Europe Beyond Coal : Europe Beyond Coal, 2022), further researches should be done on the identification of coal emissions across Europe in order to better understand its atmospheric aging processes.

References

Aas, W., Tsyro, S., Bieber, E., Bergström, R., Ceburnis, D., Ellermann, T., Fagerli, H., Frölich, M., Gehrig, R., Makkonen, U., Nemitz, E., Otjes, R., Perez, N., Perrino, C., Prévôt, A. S. H., Putaud, J. P., Simpson, D., Spindler, G., Vana, M., and Yttri, K. E.: Lessons learnt from the first EMEP intensive measurement periods, Atmos. Chem. Phys., 12(17), 8073–8094, https://doi.org/10.5194/acp-12-8073-2012, 2012.

Alfarra, M. R., Prevot, A. S. H., Szidat, S., Sandradewi, J., Weimer, S., Lanz, V. A., Schreiber, D., Mohr, M., and Baltensperger, U.: Identification of the mass spectral signature of organic aerosols from wood burning emissions, Environ. Sci. Technol., 41(16), 5770–5777, https://doi.org/10.1021/es062289b, 2007.

Allan, J. D., Delia, A. E., Coe, H., Bower, K. N., Alfarra, M. R., Jimenez, J. L., Middlebrook, A. M., Drewnick, F., Onasch, T. B., Canagaratna, M. R., Jayne, J. T., and Worsnop, D. R.: A generalised method for the extraction of chemically resolved mass spectra from Aerodyne aerosol mass spectrometer data, J. Aerosol Sci., 35(7), 909–922, https://doi.org/10.1016/j.jaerosci.2004.02.007, 2004.

Birmili, W., Heinke, K., Pitz, M., Matschullat, J., Wiedensohler, A., Cyrys, J., Wichmann, H. E., and Peters, A.: Particle number size distributions in urban air before and after volatilisation, Atmos. Chem. Phys., 10(10), 4643–4660, https://doi.org/10.5194/acp-10-4643-2010, 2010.

Birmili, W., Schepanski, K., Ansmann, A., Spindler, G., Tegen, I., Wehner, B., Nowak, A., Reimer, E., Mattis, I., M¨ Uller, K., Brüggemann, E., Brüggemann, B., Gnauk, T., Herrmann, H., Wiedensohler, A., Althausen, D., Schladitz, A., Tuch, T., and Löschau, G.: A case of extreme particulate matter concentrations over Central Europe caused by dust emitted over the southern Ukraine, Atmos. Chem. Phys., 8, www.atmos-chem-phys.net/8/997/2008/, 2008.

Birmili, W., Stratmann, F., and Wiedensohler, A.: Technical note design of a DMA-based size spectrometer for a large particle size range and stable operation, J. Aerosol Sci., 30, Issue 4, 1999.

Birmili, W., Sun, J., Wiedensohler, A., Birmili, W., Sun, J., Weinhold, K., Merkel, M., Rasch, F., Spindler, G., Wiedensohler, A., Bastian, S., Löschau, G., Schladitz, A., Quass, U., Kuhlbusch, T. A. J., Kaminski, H., Cyrys, J., Pitz, M., Gu, J., Peters, A., Flentje, H., Meinhardt, F., Schwerin, A., Bath, O., Ries, L., Gerwig, H., Wirtz, K., and Weber, S.: Enhanced Land Use Regression models for urban fine dust and ultrafine particle concentrations View project Radon parallel measurements, View project Atmospheric aerosol measurements in the German Ultrafine Aerosol Network (GUAN), https://www.researchgate.net/publication/330910927, 2015.

Birmili, W., Weinhold, K., Rasch, F., Sonntag, A., Sun, J., Merkel, M., Wiedensohler, A., Bastian, S., Schladitz, A., Löschau, G., Cyrys, J., Pitz, M., Gu, J., Kusch, T., Flentje, H., Quass, U., Kaminski, H., Kuhlbusch, T. A. J., Meinhardt, F., Schwerin, A., Bath, O., Ries, L., Gerwig, H., Wirtz, K., and Fiebig, M.: Long-term observations of tropospheric particle number size distributions and equivalent black carbon mass concentrations in the German Ultrafine Aerosol Network (GUAN), Earth System Science Data, 8(2), 355–382, https://doi.org/10.5194/essd-8-355-2016, 2016.

Birmili, W., Wiedensohler, A., Mueller, K., Birmili, W., Weinhold, K., Nordmann, S., Wiedensohler, A., Spindler, G., Müller, K., Herrmann, H., Gnauk, T., Pitz, M., Cyrys, J., Flentje, H., Nickel, C., J Kuhlbusch, T. A., Löschau, G., Haase, D., Meinhardt, F., F., Schwerin, A., Ries, L., and Wirtz, K.: Atmospheric aerosol measurements in the German Ultrafine Aerosol Network (GUAN) Korngrößendifferenzierte Feinstaubbelastung in Straßennähe in Ballungsgebieten Sachsens (2003-2005) View project Chemistry, Air Quality and Climate View project Atmospheric aerosol measurements in the German Ultrafine Aerosol Network (GUAN) Part 1: Soot and particle number size distributions, https://www.researchgate.net/publication/232089057, 2009.

Bootstrap Methods: Another Look at the Jackknife on JSTOR, https://www.jstor.org/stable/2958830?origin=JSTOR-pdf, 1979.

Bressi, M., Cavalli, F., Putaud, J. P., Fröhlich, R., Petit, J. E., Aas, W., Äijälä, M., Alastuey, A., Allan, J. D., Aurela, M., Berico, M., Bougiatioti, A., Bukowiecki, N., Canonaco, F., Crenn, V., Dusanter, S., Ehn, M., Elsasser, M., Flentje, H., M., Flentje, H., Graf, P., Green, D. C., Heikkinen, L., Hermann, H., Holzinger, R., Hueglin, C.,

24

Keernik, H., Kiendler-Scharr, A., Kubelova, L., Lunder, C., Maasikmets, M., Makes, O., Malaguti, A., Mihalopoulos, N., Nicolas, J.B., O'Dowd, C., Ovadnevaite, J., Petralia, E., Poulain, L., Priestman, M., Riffault, V., Ripoll, A., Schlag, P., Schwarz, J., Sciarec,, J., Slowik, J., Sosedova, Y., Stavroulas, I., Teinemaa, E., Via, M., Vodickar, P., Williams, P.I., Wiedensohler, A., Young, D.E., Zhang, S., Favez, O., Minguillon, M.C., and Prevot, A. S. H.: A European aerosol phenomenology - 7: High-time resolution chemical characteristics of submicron particulate matter across Europe, Atmos. Environ, X, 10, https://doi.org/10.1016/j.aeaoa.2021.100108, 2021.

Canagaratna, M. R., Jayne, J. T., Ghertner, D. A., Herndon, S., Shi, Q., Jimenez, J. L., Silva, P. J., Williams, P., Lanni, T., Drewnick, F., Demerjian, K. L., Kolb, C. E., and Worsnop, D. R.: Chase studies of particulate emissions from in-use New York City vehicles, Aerosol Sci Technol., 38(6), 555–573, https://doi.org/10.1080/02786820490465504, 2004.

Canagaratna, M. R., Jimenez, J. L., Kroll, J. H., Chen, Q., Kessler, S. H., Massoli, P., Hildebrandt Ruiz, L., Fortner, E., Williams, L. R., Wilson, K. R., Surratt, J. D., Donahue, N. M., Jayne, J. T., and Worsnop, D. R.: Elemental ratio measurements of organic compounds using aerosol mass spectrometry: Characterization, improved calibration, and implications, Atmos. Chem. Phys., 15(1), 253–272, https://doi.org/10.5194/acp-15-253-2015, 2015.

Canonaco, F., Crippa, M., Slowik, J. G., Baltensperger, U., and Prévôt, A. S. H.: SoFi, an IGOR-based interface for the efficient use of the generalized multilinear engine (ME-2) for the source apportionment: ME-2 application to aerosol mass spectrometer data, Atmos. Meas. Tech., 6(12), 3649–3661, https://doi.org/10.5194/amt-6-3649-2013, 2013.

Canonaco, F., Slowik, J. G., Baltensperger, U., and Prévôt, A. S. H.: Seasonal differences in oxygenated organic aerosol composition: Implications for emissions sources and factor analysis, Atmos. Chem. Phys., 15(12), 6993–7002, https://doi.org/10.5194/acp-15-6993-2015, 2015.

Canonaco, F., Tobler, A., Chen, G., Sosedova, Y., Gates Slowik, J., Bozzetti, C., Rudolf Daellenbach, K., el Haddad, I., Crippa, M., Huang, R. J., Furger, M., Baltensperger, U., and Prévôt, A. S. H.: A new method for long-term source apportionment with time-dependent factor profiles and uncertainty assessment using SoFi Pro: Application to 1 year of organic aerosol data. Atmos. Meas. Tech., 14(2), 923–943, https://doi.org/10.5194/amt-14-923-2021, 2021.

Canonaco, F., Tobler, A., Chen, G., Sosedova, Y., Slowik, J. G., Bozzetti, C., Daellenbach, K. R., ElHaddad, I., Crippa, M., Huang, R.-J., Furger, M., Baltensperger, U., and Prévôt, A. S. H.: A new method for long-term source apportionment with time-dependent factor profiles and uncertainty assessment using SoFi Pro: application to one year of organic aerosol data, Atmos. Meas. Tech., 1–39, https://doi.org/10.5194/amt-2020-204, 2020.

Chazeau, B., el Haddad, I., Canonaco, F., Temime-Roussel, B., D'Anna, B., Gille, G., Mesbah, B., Prévôt, A. S. H., Wortham, H., and Marchand, N.: Organic aerosol source apportionment by using rolling positive matrix factorization: Application to a Mediterranean coastal city, Atmos. Environ., X, 14, https://doi.org/10.1016/j.aeaoa.2022.100176, 2022.

Chen, G., Canonaco, F., Tobler, A., Aas, W., Alastuey, A., Allan, J., Atabakhsh, S., Aurela, M., Baltensperger, U., Bougiatioti, A., de Brito, J. F., Ceburnis, D., Chazeau, B., Chebaicheb, H., Daellenbach, K. R., Ehn, M., el Haddad, I., Eleftheriadis, K., Favez, O., Flentje, H., Font, A., Fossum, K., Freney, E., Gini, M., Green, D.C., Heikkinen, L., Herrmann, H., Kalogridis, A., Keernik, H., Lhotka, R., Lin, C., Lunder, C., Maasikmets, M., Manousakas, M.I., Marchand, N., Marin, C., Marmureanu, L., Mihalopoulos, N., Mocnika, G., Nęckia, J., O'Dowd, C., Ovadnevaite, J., Petera, T., Petita, J.E., Pikridasa, M., Matthew Platt, S., Pokorna, P., Poulain, L., Priestman, M., Riffault, V., Rinaldia, M., Rozanskia, K., Schwarz, J., Sciarea, J., Simon, L., Skiba, A., Slowik, J.G., Sosedova, Y., Stavroulas, I., Styszkoa, K., Teinemaa, E., Timonen, H., Tremper, A., Vasilescu, J., Via, M., Vodicka, P., Wiedensohler, A., Zografou, O., Cruz Minguillon, M., and Prévôt, A. S. H.: European aerosol phenomenology − 8: Harmonised source apportionment of organic aerosol using 22 Year-long ACSM/AMS datasets, Environ. Int., 166, https://doi.org/10.1016/j.envint.2022.107325, 2022.

Chen, G., Sosedova, Y., Canonaco, F., Fröhlich, R., Tobler, A., Vlachou, A., Daellenbach, K., Bozzetti, C., Hueglin, C., Graf, P., Baltensperger, U., Slowik, J., el Haddad, I., and Prévôt, A.: Time dependent source apportionment of submicron organic aerosol for a rural site in an alpine valley using a rolling PMF window, Atmos. Chem. Phys., 1–52, https://doi.org/10.5194/acp-2020-1263, 2020.

Chen, G., Sosedova, Y., Canonaco, F., Fröhlich, R., Tobler, A., Vlachou, A., Daellenbach, K. R., Bozzetti, C., Hueglin, C., Graf, P., Baltensperger, U., Slowik, J. G., el Haddad, I., and Prévôt, A. S. H.: Time-dependent source apportionment of submicron organic aerosol for a rural site in an alpine valley using a rolling positive matrix factorisation (PMF) window, Atmos. Chem. Phys., 21(19), 15081–15101, https://doi.org/10.5194/acp-21-15081-2021, 2021.

Crippa, M., Canonaco, F., Lanz, V. A., Äijälä, M., Allan, J. D., Carbone, S., Capes, G., Ceburnis, D., Dall'Osto, M., Day, D. A., DeCarlo, P. F., Ehn, M., Eriksson, A., Freney, E., Ruiz, L. H., Hillamo, R., Jimenez, J. L., Junninen, H., Kiendler-Scharr, A., Kortelainen, A.-M., Kulmala, M., Laaksonen, A., Mensah10, A.A., Mohr1, C., Nemitz, E., O'Dowd, C., Ovadnevaite, J., Pandis, S. N., Petäjä, T., Poulain, L., Saarikoski, S., Sellegri, K., Swietlicki, E., Tiitta, P., Worsnop, D. R., Baltensperger, U., and Prévôt, A. S. H.: Organic aerosol components derived from 25 AMS data sets across Europe using a consistent ME-2 based source apportionment approach. Atmos. Chem. Phys., 14(12), 6159–6176, https://doi.org/10.5194/acp-14-6159-2014, 2014.

Crippa, M., Decarlo, P. F., Slowik, J. G., Mohr, C., Heringa, M. F., Chirico, R., Poulain, L., Freutel, F., Sciare, J., Cozic, J., di Marco, C. F., Elsasser, M., Nicolas, J. B., Marchand, N., Abidi, E., Wiedensohler, A., Drewnick, F., Schneider, J., Borrmann, S., Nemitz, E., Zimmermann, R., Jaffrezo, J.-L., Prevot, A. S. H., and Baltensperger, U. Wintertime aerosol chemical composition and source apportionment of the organic fraction in the metropolitan area of Paris, Atmos. Chem. Phys., 13(2), 961–981, https://doi.org/10.5194/acp-13-961-2013, 2013.

Daellenbach, K. R., Uzu, G., Jiang, J., Cassagnes, L. E., Leni, Z., Vlachou, A., Stefenelli, G., Canonaco, F., Weber, S., Segers, A., Kuenen, J. J. P., Schaap, M., Favez, O., Albinet, A., Aksoyoglu, S., Dommen, J., Baltensperger, U.,

Geiser, M., el Haddad, I., Jaffrezo, J.L., and Prévôt, A. S. H.: Sources of particulate-matter air pollution and its oxidative potential in Europe, Nature, 587(7834), 414–419, https://doi.org/10.1038/s41586-020-2902-8, 2020.

Dall'Osto, M., Ovadnevaite, J., Ceburnis, D., Martin, D., Healy, R. M., O'Connor, I. P., Kourtchev, I., Sodeau, J. R., Wenger, J. C., and O'Dowd, C.: Characterization of urban aerosol in Cork city (Ireland) using aerosol mass spectrometry. Atmos. Chem. Phys., 13(9), 4997–5015, https://doi.org/10.5194/acp-13-4997-2013, 2013.

Draxler, R.R. and Hess, G.D.: Description of the HYSPLIT-4 Modeling System, NOAA Technical Memorandum ERL ARL-224, NOAA Air Resources Laboratory, Silver Spring, 1-24, 1997.

Dudoitis, V., Byčenkiene, S., Plauškaite, K., Bozzetti, C., Fröhlich, R., Mordas, G., and Ulevičius, V.: Spatial distribution of carbonaceous aerosol in the southeastern Baltic Sea region (event of grass fires), Acta Geophysica, 64(3), 711–731, https://doi.org/10.1515/acgeo-2016-0018, 2016.

Energy statistics - an overview - Statistics Explained, https://ec.europa.eu/eurostat/statistics-explained/index.php?title=Energy_statistics_-_an_overview, 2022.

Europe's coal exit - Europe Beyond Coal: Europe Beyond Coal, https://beyond-coal.eu/europes-coal-exit/, 2022.

Fröhlich, R., Crenn, V., Setyan, A., Belis, C. A., Canonaco, F., Favez, O., Riffault, V., Slowik, J. G., Aas, W., Aijälä, M., Alastuey, A., Artiñano, B., Bonnaire, N., Bozzetti, C., Bressi, M., Carbone, C., Coz, E., Croteau, P. L., Cubison, M. J., Esser-Gietl, J. K., Green, D. C., Gros, V., Heikkinen, L., Herrmann, H., Jayne, J. T., Lunder, C. R., Minguillón, M. C., Mocnik, G., O'Dowd, C. D., Ovadnevaite, J., Petralia, E., Poulain, L., Priestman, M., Ripol, Sarda-Estève, A., R., Wiedensohler, A., Baltensperger, U., Sciare, J., and Prévôt, A. S. H., ACTRIS ACSM intercomparison - Part 2: Intercomparison of ME-2 organic source apportionment results from 15 individual, co-located aerosol mass spectrometers, Atmos. Meas. Tech., 8(6), 2555–2576, https://doi.org/10.5194/amt-8-2555-2015, 2015.

Fröhlich, R., Cubison, M. J., Slowik, J. G., Bukowiecki, N., Prévôt, A. S. H., Baltensperger, U., Schneider, J., Kimmel, J. R., Gonin, M., Rohner, U., Worsnop, D. R., and Jayne, J. T.: The ToF-ACSM: A portable aerosol chemical speciation monitor with TOFMS detection. Atmos. Meas. Tech., 6(11), 3225–3241, https://doi.org/10.5194/amt-6-3225-2013, 2013.

Gilardoni, S., Massoli, P., Paglione, M., Giulianelli, L., Carbone, C., Rinaldi, M., Decesari, S., Sandrini, S., Costabile, F., Gobbi, G. P., Pietrogrande, M. C., Visentin, M., Scotto, F., Fuzzi, S., and Facchini, M. C.: Direct observation of aqueous secondary organic aerosol from biomass-burning emissions, Proceedings of the National Academy of Sciences of the United States of America, 113(36), 10013–10018, https://doi.org/10.1073/pnas.1602212113, 2016.

Heikkinen, L., Äijälä, M., Daellenbach, K., Chen, G., Garmash, O., Aliaga, D., Graeffe, F., Räty, M., Luoma, K., Aalto, P., Kulmala, M., Petäjä, T., Worsnop, D., and Ehn, M.: Eight years of sub-micrometre organic aerosol composition data from the boreal forest characterized using a machine-learning approach, Atmos. Chem. Phys., 1–47, https://doi.org/10.5194/acp-2020-868, 2020.

Henry, R., Norris, G. A., Vedantham, R., and Turner, J. R.: Source region identification using kernel smoothing, Environ. Sci. Technol., 43(11), 4090–4097, https://doi.org/10.1021/es8011723, 2009.

Huang, S., Wu, Z., Poulain, L., van Pinxteren, M., Merkel, M., Assmann, D., Herrmann, H., and Wiedensohler, A.: Source apportionment of the organic aerosol over the Atlantic Ocean from 53°N to 53°S: Significant contributions from marine emissions and long-range transport, Atmos. Chem. Phys., 18(24), 18043–18062, https://doi.org/10.5194/acp-18-18043-2018, 2018.

Huang, W., Saathoff, H., Shen, X., Ramisetty, R., Leisner, T., and Mohr, C.: Seasonal characteristics of organic aerosol chemical composition and volatility in Stuttgart, Germany, Atmos. Chem. Phys., 19(18), 11687–11700, https://doi.org/10.5194/acp-19-11687-2019, 2019.

Hussein, T., Karppinen, A., Kukkonen, J., Härkönen, J., Aalto, P. P., Hämeri, K., Kerminen, V. M., and Kulmala, M.: Meteorological dependence of size-fractionated number concentrations of urban aerosol particles, Atmos. Environ., 40(8), 1427–1440, https://doi.org/10.1016/j.atmosenv.2005.10.061, 2006.

Iapalucci, T. L., Demski, R. J., and Bienstock, D.: Chlorine in Coal Combustion. United States Department of the Interior, Bureau of Mines Report of Investigation 7260s, 1969.

Iinuma, Y., Engling, G., Puxbaum, H., and Herrmann, H.: A highly resolved anion-exchange chromatographic method for determination of saccharidic tracers for biomass combustion and primary bio-particles in atmospheric aerosol, Atmos. Environ., 43(6), 1367–1371, https://doi.org/10.1016/j.atmosenv.2008.11.020, 2009.

Jayne, J. T., Leard, D. C., Zhang, X., Davidovits, P., Smith, K. A., Kolb, C. E., and Worsnop, D. R.: Development of an Aerosol Mass Spectrometer for Size and Composition Analysis of Submicron Particles, Aerosol Sci Technol., 33:1-2, 48-70, https://doi.org/10.1080/027868200410840, 2000.

Jimenez, J. L., Canagaratna, M. R., Donahue, N. M., Prevot, A. S. H., Zhang, Q., Kroll, J. H., DeCarlo, P. F., Allan, J. D., Coe, H., Ng, N. L., Aiken, A. C., Docherty, K. S., Ulbrich, I. M., Grieshop, A. P., Robinson, A. L., Duplissy, J., Smith, J. D., Wilson, K. R., Lanz, V. A., Hueglin, C., Sun, Y. L., Tian, J., Laaksonen, A., Raatikainen, T., Rautiainen, J., Vaattovaara, P., Ehn, M., Kulmala, M., Tomlinson, J. M., Collins, D. R., Cubison, M. J., Dunlea, E. J., Huffman, J. A., Onasch, T. B., Alfarra, M. R., Williams, P. I., Bower, K., Kondo, Y., Schneider, J., Drewnick, F., Borrmann, S., Weimer, S., Demerjian, K., Salcedo, D., Cottrell, L., Griffin, R., Takami, A., Miyoshi, T., Hatakeyama, S., Shimono, A., Sun, J. Y, Zhang, Y. M., Dzepina, K., Kimmel, J. R., Sueper, D., Jayne, J. T., Herndon, S. C., Trimborn, A. M., Williams, L. R., Wood, E. C., Middlebrook, A. M., Kolb, C. E., Baltensperger, U., and Worsnop, D. R.: Evolution of organic aerosols in the atmosphere. Science, 326(5959), 1525–1529, https://doi.org/10.1126/science.1180353, 2009.

Katsanos, D., Bougiatioti, A., Liakakou, E., Kaskaoutis, D. G., Stavroulas, I, Paraskevopoulou, D., Lianou, M., Psiloglou, B. E., Gerasopoulos, E., Pilinis, C., and Mihalopoulos, N.: Optical properties of near-surface urban aerosols and their chemical tracing in a mediterranean city (Athens), Aerosol and Air Quality Research, 19(1), 49–70, https://doi.org/10.4209/aaqr.2017.11.0544, 2019.

Keck, L. and Wittmaack, K.: Effect of filter type and temperature on volatilisation losses from ammonium salts in aerosol matter, Atmos. Environ., 39, 4093–4100, https://doi.org/10.1016/j.atmosenv.2005.03.029, 2005.

Kiendler-Scharr, A., Mensah, A. A., Friese, E., Topping, D., Nemitz, E., Prevot, A. S. H., Äijälä, M., Allan, J., Canonaco, F., Canagaratna, M., Carbone, S., Crippa, M., Dall Osto, M., Day, D. A., de Carlo, P., di Marco, C. F., Elbern, H., Eriksson, A., Freney, E., Hao, L., Herrmann, H., Hildebrandt, L.,. Hillamo, R., Jimenez, J. L., Laaksonen, A., McFiggans, G., Mohr, C., O'Dowd, C., Otjes, R., Ovadnevaite, J., Pandis, S. N., Poulain, L., Schlag, P., Sellegri, K., Swietlicki, E., Tiitta, P., Vermeulen, A., Wahner, A., Worsnop, D. and Wu, H. C.: Ubiquity of organic nitrates from night time chemistry in the European submicron aerosol, Geophysical Research Letters, 43(14), 7735–7744, https://doi.org/10.1002/2016GL069239, 2016.

Kodros, J., Papanastasiou, D., Paglionea, M., Masiol, M., Squizzato, S., Florou, K., Skyllakou, K., Kaltsonoudis, C., Nenesa, A., and Pandisa, S.: Rapid dark aging of biomass burning as an overlookedsource of oxidized organic aerosol, PNAS, https://doi.org/10.1073/pnas.1602212113, 2020.

Kumar, V., Giannoukos, S., Haslett, S. L., Tong, Y., Singh, A., Bertrand, A., Lee, C. P., Wang, D. S., Bhattu, D., Stefenelli, G., Dave, J. S., Puthussery, J. v., Qi, L., Vats, P., Rai, P., Casotto, R., Satish, R., Mishra, S., Pospisilova, V., C., Bell, D.M., Ganguly, D., Verma, V., Rastogi, N., Baltensperger, U., Tripathi, S.N., Prévôt, A.S.H., and Slowik, J. G.: Highly time-resolved chemical speciation and source apportionment of organic aerosol components in Delhi, India, using extractive electrospray ionization mass spectrometry, Atmos. Chem. Phys., 22(11), 7739–7761, https://doi.org/10.5194/acp-22-7739-2022, 2022.

Laborde, M., Crippa, M., Tritscher, T., Jurányi, Z., Decarlo, P. F., Temime-Roussel, B., Marchand, N., Eckhardt, S., Stohl, A., Baltensperger, U., Prévôt, A. S. H., Weingartner, E., and Gysel, M.: Black carbon physical properties and mixing state in the European megacity Paris, Atmos. Chem. Phys., 13(11), 5831–5856, https://doi.org/10.5194/acp-13-5831-2013, 2013.

Lanz, V., Prevot, A., Alfarra, M., Weimer, S., Mohr, C., DeCarlo, P., Gianini, M., Hueglin, C., Schneider, J., Favez, O., D'Anna, B., George, C., and Baltensperger, U.: Characterization of aerosol chemical composition with aerosol massspectrometry in Central Europe: an overview, Atmos. Chem. Phys., 10, 10453–10471, 2010.

Li, G., Lei, W., Bei, N., and Molina, L. T.: Contribution of garbage burning to chloride and PM 2.5 in Mexico City, Atmos. Chem. Phys., 12(18), 8751–8761, https://doi.org/10.5194/acp-12-8751-2012, 2012.

Lin, C., Ceburnis, D., Hellebust, S., Buckley, P., Wenger, J., Canonaco, F., Prévôt, A. S. H., Huang, R. J., O'Dowd, C., and Ovadnevaite, J.: Characterization of Primary Organic Aerosol from Domestic Wood, Peat, and Coal Burning in Ireland, Environ. Sci. Technol., 51(18), 10624–10632, https://doi.org/10.1021/acs.est.7b01926, 2017.

Liu, P. S. K., Deng, R., Smith, K. A., Williams, L. R., Jayne, J. T., Canagaratna, M. R., Moore, K., Onasch, T. B., Worsnop, D. R., and Deshler, T.: Transmission efficiency of an aerodynamic focusing lens system: Comparison of model calculations and laboratory measurements for the aerodyne aerosol mass spectrometer, Aerosol Sci Technol., 41(8), 721–733, https://doi.org/10.1080/02786820701422278, 2007.

Ma, N., Birmili, W., Müller, T., Tuch, T., Cheng, Y. F., Xu, W. Y., Zhao, C. S., and Wiedensohler, A.: Tropospheric aerosol scattering and absorption over central Europe: A closure study for the dry particle state. Atmos. Chem. Phys., 14(12), 6241–6259, https://doi.org/10.5194/acp-14-6241-2014, 2014.

Marin, C., Marmureanu, L., Rado, C., Dodosci, A., Stan, C., Toanca, F., Preda, L., and Antonescu, B.: Wintertime Variations of Gaseous Atmospheric Constutuents in Bucharest Peri-Urban Area, Atmosphere, 10(8), 478; https://doi.org/10.3390/atmos10080478, 2019.

Middlebrook, A. M., Bahreini, R., Jimenez, J. L., and Canagaratna, M. R.: Evaluation of composition-dependent collection efficiencies for the Aerodyne aerosol mass spectrometer using field data. Aerosol Sci Technol., 46(3), 258–271, https://doi.org/10.1080/02786826.2011.620041, 2012.

Ng, N. L., Canagaratna, M. R., Zhang, Q., Jimenez, J. L., Tian, J., Ulbrich, I. M., Kroll, J. H., Docherty, K. S., Chhabra, P. S., Bahreini, R., Murphy, S. M., Seinfeld, J. H., Hildebrandt, L., Donahue, N. M., Decarlo, P. F., Lanz, V. A., Prévôt, A. S. H., Dinar, E., Rudich, Y., and Worsnop, D. R.: Organic aerosol components observed in Northern Hemispheric datasets from Aerosol Mass Spectrometry, Atmos. Chem. Phys., 10(10), 4625–4641, https://doi.org/10.5194/acp-10-4625-2010, 2010.

Ng, N. L., Herndon, S. C., Trimborn, A., Canagaratna, M. R., Croteau, P. L., Onasch, T. B., Sueper, D., Worsnop, D. R., Zhang, Q., Sun, Y. L., and Jayne, J. T.: An Aerosol Chemical Speciation Monitor (ACSM) for routine monitoring of the composition and mass concentrations of ambient aerosol, Aerosol Sci Technol., 45(7), 780–794, https://doi.org/10.1080/02786826.2011.560211, 2011.

O'Dowd, C., Ceburnis, D., Ovadnevaite, J., Vaishya, A., Rinaldi, M., and Facchini, M. C.: Do anthropogenic, continental or coastal aerosol sources impact on a marine aerosol signature at Mace Head? Atmos. Chem. Phys., 14(19), 10687–10704, https://doi.org/10.5194/acp-14-10687-2014, 2014.

Ovadnevaite, J., Ceburnis, D., Leinert, S., Dall'Osto, M., Canagaratna, M., O'Doherty, S., Berresheim, H., and O'Dowd, C.: Submicron NE Atlantic marine aerosol chemical composition and abundance: Seasonal trends and air mass categorization, J. Geophys. Res., 119(20), 11,850-11,863, https://doi.org/10.1002/2013JD021330, 2014.

Paatero, P.: Least squares formulation of robust non-negative factor analysis, In Chemometrics and Intelligent Laboratory Systems, 37, 1997.

Paatero, P.: The Multilinear Engine- A Table-Driven, Least Squares Program for Solving Multilinear Problems, Including the n-Way Parallel Factor Analysis Model, J Comput Graph Stat., 8(4), 854–888, https://doi.org/10.1080/10618600.1999.10474853, 1999.

Paatero, P., and Tappert, U.: Positive matrix factorization: A non-negative factor model with optimal utilization of error estimates of data values *, ENVIRONMETRICS, 5, 111-126, 1994.

Paglione, M., Gilardoni, S., Rinaldi, M., Decesari, S., Zanca, N., Sandrini, S., Giulianelli, L., Bacco, D., Ferrari, S., Poluzzi, V., Scotto, F., Trentini, A., Poulain, L., Herrmann, H., Wiedensohler, A., Canonaco, F., Prévôt, A. S. H., Massoli, P., Carbone, C., C., Bell, D.M., Ganguly, D., Verma, V., Rastogi, N., Baltensperger, U., Tripathi, S.N.,

Prévôt, A.S.H., and Fuzzi, S.: The impact of biomass burning and aqueous-phase processing on air quality: A multi-year source apportionment study in the Po Valley, Italy, Atmos. Chem. Phys., 20(3), 1233–1254, https://doi.org/10.5194/acp-20-1233-2020, 2020.

Parworth, C., Fast, J., Mei, F., Shippert, T., Sivaraman, C., Tilp, A., Watson, T., and Zhang, Q.: Long-term measurements of submicrometer aerosol chemistry at the Southern Great Plains (SGP) using an Aerosol Chemical Speciation Monitor (ACSM), Atmos. Environ., 106, 43–55, https://doi.org/10.1016/j.atmosenv.2015.01.060, 2015.

Petit, J.-E., Favez, O., Sciare, J., Crenn, V., Sarda-Esteve, R., Bonnaire, N., Mocnik, G., Dupont, J. C., Haeffelin, M., Leoz-Garziandia, E., Sarda, R., Petit, J.-E., Favez, O., Sciare, J., Crenn, V., Sarda-Estève, R., Bonnaire, N., Močnik, G., Dupont, J.-C., Haeffelin., M., and Leoz-Garziandia, E.: Two years of near real-time chemical composition of submicron aerosols in the region of Paris using an Aerosol Chemical Speciation Monitor (ACSM) and a multi-wavelength Aethalometer, European Geosciences Union, 15(6), 2985–3005, https://doi.org/10.5194/acpd-14-24221-2014ï, 2015.

Petzold, A., and Schönlinner, M.: Multi-angle absorption photometry - A new method for the measurement of aerosol light absorption and atmospheric black carbon, J. Aerosol Sci., 35(4), 421–441, https://doi.org/10.1016/j.jaerosci.2003.09.005, 2004.

Pope, C. A., and Dockery, D. W., Health Effects of Fine Particulate Air Pollution: Lines that Connect, J. Air & Waste Manage. Assoc 56, 35, https://doi.org/10.1080/10473289.2006.10464485 2006.

Poulain, L., Birmili, W., Canonaco, F., Crippa, M., Wu, Z. J., Nordmann, S., Spindler, G., Prévôt, A. S. H., Wiedensohler, A., and Herrmann, H.: Chemical mass balance of 300 °c non-volatile particles at the tropospheric research site Melpitz, Germany, Atmos. Chem. Phys., 14(18), 10145–10162, https://doi.org/10.5194/acp-14-10145-2014, 2014.

Poulain, L., Fahlbusch, B., Spindler, G., Müller, K., van Pinxteren, D., Wu, Z., Iinuma, Y., Birmili, W., Wiedensohler, A., and Herrmann, H.: Source apportionment and impact of long-range transport on carbonaceous aerosol particles in central Germany during HCCT-2010, Atmos. Chem. Phys., 21(5), 3667–3684, https://doi.org/10.5194/acp-21-3667-2021, 2021.

Poulain, L., Spindler, G., Birmili, W., Plass-Dülmer, C., Wiedensohler, A., and Herrmann, H.: Seasonal and diurnal variations of particulate nitrate and organic matter at the IfT research station Melpitz. Atmos. Chem. Phys., 11(24), 12579–12599, https://doi.org/10.5194/acp-11-12579-2011, 2011.

Poulain, L., Spindler, G., Grüner, A., Tuch, T., Stieger, B., Pinxteren, D. van, Petit, J. E., Favez, O., Herrmann, H., and Wiedensohler, A.: Multi-year ACSM measurements at the central European research station Melpitz (Germany)- Part 1: Instrument robustness, quality assurance, and impact of upper size cutoff diameter, Atmos. Meas. Tech., 13(9), 4973–4994, https://doi.org/10.5194/amt-13-4973-2020, 2020.

Qi, L., Vogel, A. L., Esmaeilirad, S., Cao, L., Zheng, J., Jaffrezo, J. L., Fermo, P., Kasper-Giebl, A., Daellenbach, K. R., Chen, M., Ge, X., Baltensperger, U., Prévôt, A. S. H., and Slowik, J. G.: A 1-year characterization of organic aerosol composition and sources using an extractive electrospray ionization time-of-flight mass spectrometer (EESI-TOF), Atmos. Chem. Phys., 20(13), 7875–7893, https://doi.org/10.5194/acp-20-7875-2020, 2020.

Saha, P., Kylystov, A., and Grieshop, A.: Downwind evolution of the volatility and mixing state of near-road aerosols near a US interstate highway, ACP, https://doi.org/10.5194/acp-18-2139, 2018.

Schaap, M., Spindler, G., Schulz, M., Acker, K., Maenhaut, W., Berner, A., Wieprecht, W., Streit, N., Muller, K., Bruggemann, E., Chi, X., Putaud, J. P., Hitzenberger, R., Puxbaum, H., Baltensperger, U., and ten Brink, H.: Artefacts in the sampling of nitrate studied in the "INTERCOMP" campaigns of EUROTRAC-AEROSOL, Atmos. Environ., 38, 6487–6496, https://doi.org/10.1016/j.atmosenv.2004.08.026, 2004.

Schlag, P., Kiendler-Scharr, A., Johannes Blom, M., Canonaco, F., Sebastiaan Henzing, J., Moerman, M., Prévôt, A. S. H., and Holzinger, R.: Aerosol source apportionment from 1-year measurements at the CESAR tower in Cabauw, the Netherlands, Atmos. Chem. Phys., 16(14), 8831–8847, https://doi.org/10.5194/acp-16-8831-2016, 2016.

Schmale, J., Henning, S., Henzing, B., Keskinen, H., Sellegri, K., Ovadnevaite, J., Bougiatioti, A., Kalivitis, N., Stavroulas, I., Jefferson, A., Park, M., Schlag, P., Kristensson, A., Iwamoto, Y., Pringle, K., Reddington, C., Aalto, P., Äijälä, M., Baltensperger, U., Bialek, J., Birmili, W., Bukowiecki, N., Ehn, M., Fjæraa, A., Fiebig, M., Frank, G., Fröhlich, R., Frumau, A., Furuya, M., Hammer, E., Heikkinen, L., Herrmann, E., Holzinger, R., Hyono, H., Kanakidou, M., Kiendler-Scharr, A., Kinouchi, K., Kos, G., Kulmala, M., Mihalopoulos, N., Motos, G., Nenes, A., O'Dowd, C., Paramonov, M., Petäjä, T., Picard, D., Poulain, L., Prévôt, A., Slowik, J., Sonntag, A., Swietlicki, E., Svenningsson, B., Tsurumaru, H., Wiedensohler, A., Wittbom, C., Ogren, J., Matsuki, A., Yum, S., Myhre, G., Carslaw, K., Stratmann F., and Gysel, M.: Collocated observations of cloud condensation nuclei, particle size distributions, and chemical composition. Sci Data 4, 170003, https://doi.org/10.1038/sdata.2017.3, 2017.

Seinfeld, J. H., and Pandis, S. N.: Atmospheric Chemistry and Physics: From Air Pollution to Climate Change, 3rd Edition, 1152, ISBN 9781118947401, 2006.

Shi, Y., Chen, J., Hu, D., Wang, L., Yang, X., and Wang, X.: Airborne submicron particulate (PM1) pollution in Shanghai, China: Chemical variability, formation/dissociation of associated semi-volatile components and the impacts on visibility, Science of the Total Environment, 473–474, 199–206, https://doi.org/10.1016/j.scitotenv.2013.12.024, 2014.

Shrivastava, M., Cappa, C. D., Fan, J., Goldstein, A. H., Guenther, A. B., Jimenez, J. L., Kuang, C., Laskin, A., Martin, S. T., Ng, N. L., Petaja, T., Pierce, J. R., Rasch, P. J., Roldin, P., Seinfeld, J. H., Shilling, J., Smith, J. N., Thornton, J. A., Volkamer, R., Wang, J., Worsnop, D.R., Zaveri, R.A., Zelenyuk, A., and Zhang, Q.: Recent advances in understanding secondary organic aerosol: Implications for global climate forcing, Reviews of Geophysics, 55(2), 509–559, https://doi.org/10.1002/2016RG000540, 2017.

Simoneit, B. R. T., and Elias, V. O.: Detecting Organic Tracers from Biomass Burning in the Atmosphere, Marine Pollution Bulletin, 42, 10, 805-810, DOI: 10.1016/s0025-326x(01)00094-7, 2001.

Simoneit, B. R. T., Schauer, J. J., Nolte, C. G., Oros, D. R., Elias, V. O., Fraser, M. P., Rogge, W. F., and Cass, G. R.: Levoglucosan, a tracer for cellulose in biomass burning and atmospheric particles, Atmos. Environ., 33, 173-182, https://doi.org/10.1016/S1352-2310(98)00145-9, 1999.

Spindler, G., Brüggemann, E., Gnauk, T., Grüner, A., Müller, K., and Herrmann, H.: A four-year size-segregated characterization study of particles PM10, PM2.5 and PM1 depending on air mass origin at Melpitz, Atmos. Environ., 44(2), 164–173, https://doi.org/10.1016/j.atmosenv.2009.10.015, 2010.

Spindler, G., Gnauk, T., Grüner, A., Iinuma, Y., Müller, K., Scheinhardt, S., and Herrmann, H.: Size-segregated characterization of PM10 at the EMEP site Melpitz (Germany) using a five-stage impactor: A six-year study, J. Atmos. Chem., 69(2), 127–157, https://doi.org/10.1007/s10874-012-9233-6, 2012.

Spindler, G., Grüner, A., Müller, K., Schlimper, S., and Herrmann, H.: Long-term size-segregated particle (PM10, PM2.5, PM1) characterization study at Melpitz - Influence of air mass inflow, weather conditions and season, J. Atmos. Chem., 70(2), 165–195, https://doi.org/10.1007/s10874-013-9263-8, 2013.

Spindler, G., Müller, K., Brüggemann, E., Gnauk, T., and Herrmann, H.: Long-term size-segregated characterization of PM 10, PM 2.5, and PM$_1$ at the IfT research station Melpitz downwind of Leipzig (Germany) using high and low-volume filter samplers, Atmos. Environ., 38(31), 5333–5347, https://doi.org/10.1016/j.atmosenv.2003.12.047, 2004.

Stavroulas, I., Bougiatioti, A., Grivas, G., Paraskevopoulou, D., Tsagkaraki, M., Zarmpas, P., Liakakou, E., Gerasopoulos, E., and Mihalopoulos, N.K: Sources and processes that control the submicron organic aerosol composition in an urban Mediterranean environment (Athens): A high temporal-resolution chemical composition measurement study, Atmos. Chem. Phys., 19(2), 901–919, https://doi.org/10.5194/acp-19-901-2019, 2019.

Stieger, B., Spindler, G., Fahlbusch, B., Müller, K., Grüner, A., Poulain, L., Thöni, L., Seitler, E., Wallasch, M., and Herrmann, H.: Measurements of PM10 ions and trace gases with the online system MARGA at the research station Melpitz in Germany – A five-year study, J. Atmos. Chem., 75(1), 33–70, https://doi.org/10.1007/s10874-017-9361-0, 2018.

Sun, J., Birmili, W., Hermann, M., Tuch, T., Weinhold, K., Merkel, M., Rasch, F., Müller, T., Schladitz, A., Bastian, S., Löschau, G., Cyrys, J., Gu, J., Flentje, H., Briel, B., Asbach, C., Kaminski, H., Ries, L., Sohmer, R., Gerwig, H., Wirtz, K., Meinhardt, F., Schwerin, A., Bath, O., Ma, N., and Wiedensohler, A.: Decreasing trends of particle number and black carbon mass concentrations at 16 observational sites in Germany from 2009 to 2018, Atmos. Chem. Phys., 20(11), 7049–7068, https://doi.org/10.5194/acp-20-7049-2020, 2020.

Sun, Y., Xu, W., Zhang, Q., Jiang, Q., Canonaco, F., Prévôt, A. S. H., Fu, P., Li, J., Jayne, J., Worsnop, D. R., and Wang, Z.: Source apportionment of organic aerosol from 2-year highly time-resolved measurements by an aerosol

chemical speciation monitor in Beijing, China, Atmos. Chem. Phys., 18(12), 8469–8489, https://doi.org/10.5194/acp-18-8469-2018, 2018.

Tiitta, P., Leskinen, A., Hao, L., Yli-Pirilä, P., Kortelainen, M., Grigonyte, J., Tissari, J., Lamberg, H., Hartikainen, A., Kuuspalo, K., Kortelainen, A. M., Virtanen, A., Lehtinen, K. E. J., Komppula, M., Pieber, S., Prévôt, A. S. H., Onasch, T. B., Worsnop, D. R., Czech, H., Zimmermann, R., Jokiniemi, J., and Sippula, O.: Transformation of logwood combustion emissions in a smog chamber: Formation of secondary organic aerosol and changes in the primary organic aerosol upon daytime and night time aging, Atmos. Chem. Phys., 16(20), 13251–13269, https://doi.org/10.5194/acp-16-13251-2016, 2016.

Tobler, A., Skiba, A., Canonaco, F., Močnik, G., Rai, P., Chen, G., Bartyzel, J., Zimnoch, M., Styszko, K., Nęcki, J., Furger, M., Różański, K., Baltensperger, U., Slowik, J., and Prévôt, A.: Characterization of NR-PM1 and source apportionment of organic aerosol in Krakow, Poland, Atmos. Chem. Phys., 1–22, https://doi.org/10.5194/acp-2021-197, 2021.

Ulbrich, I. M., Canagaratna, M. R., Zhang, Q., Worsnop, D. R., and Jimenez, J. L.: Interpretation of organic components from Positive Matrix Factorization of aerosol mass spectrometric data, Atmos. Chem. Phys., 9, www.atmos-chem-phys.net/9/2891/2009/, 2009.

van Pinxteren, D., Fomba, K. W., Spindler, G., Müller, K., Poulain, L., Iinuma, Y., Löschau, G., Hausmann, A., and Herrmann, H.; Regional air quality in Leipzig, Germany: Detailed source apportionment of size-resolved aerosol particles and comparison with the year 2000, Faraday Discussions, 189, 291–315, https://doi.org/10.1039/c5fd00228a, 2016.

van Pinxteren, D., Mothes, F., Spindler, G., Fomba, K. W., Cuesta, A., Tuch, T., Müller, T., Wiedensohler, A., and Herrmann, H.: Zusatzbelastung aus Holzheizung, Sächsisches Landesamt für Umwelt, Landwirtschaft und Geologie (LfULG), Dresden, https://publikationen.sachsen.de/bdb/artikel/36106, 2020.

Via, M., Minguillón, M. C., Reche, C., Querol, X., and Alastuey, A.: Increase of secondary organic aerosol over four years in an urban environment, Atmos. Chem. Phys., 1–20, https://doi.org/10.5194/acp-2020-1244, 2020.

Vlachou, A., Daellenbach, K., Bozzetti, C., Chazeau, B., Salazar, G., Szidat, S., Jaffrezo, J.-L., Hueglin, C., Baltensperger, U., Haddad, I. el, Daellenbach, K. R., Salazar, G. A., and Prévôt, A. S. H.: Advanced source apportionment of carbonaceous aerosols by coupling offline AMS and radiocarbon size-segregated measurements over a nearly 2-year period, Atmos. Chem. Phys., 18(9), 6187–6206, https://doi.org/10.5194/acp-18-6187-2018ï, 2018.

Vlachou, A., Tobler, A., Lamkaddam, H., Canonaco, F., Daellenbach, K. R., Jaffrezo, J. L., Minguillón, M. C., Maasikmets, M., Teinemaa, E., Baltensperger, U., el Haddad, I., and Preávôt, A. S. H.: Development of a versatile source apportionment analysis based on positive matrix factorization: a case study of the seasonal variation of organic aerosol sources in Estonia, Atmos. Chem. Phys., 19(11), 7279–7295, https://doi.org/10.5194/acp-19-7279-2019, 2019.

Wang, Y., Henning, S., Poulain, L., Lu, C., Stratmann, F., Wang, Y., Niu, S., Pöhlker, M., Herrmann, H., and Wiedensohler, A.: Aerosol activation characteristics and prediction at the central European ACTRIS research station of Melpitz, Germany, https://doi.org/10.5194/acp-22-15943, 2022.

Wang, T., Fu, T., Chen, K., Cheng, R., Chen, S., Liu, J., Mei, M., Li, J., and Xue, Y.: Co-combustion behavior of dyeing sludge and rice husk by using TG-MS: Thermal conversion, gas evolution, and kinetic analyses, Bioresource Technology, 311, https://doi.org/10.1016/j.biortech.2020.123527, 2020.

Watson, J. G.: Visibility: science and regulation, J. Air Waste Manage., 52, 628-713, https://doi.org/10.1080/10473289.2002.10470813, 2002.

Wehner, B., Philippin, S., and Wiedensohler, A.: Design and calibration of a thermodenuder with an improved heating unit to measure the size-dependent volatile fraction of aerosol particles, Aerosol Science, 33, www.elsevier.com/locate/jaerosci, 2002.

WHO, Expert Consultation: https://www.who.int/news-room/events/detail/2019/02/12/default-calendar/expert-consultation-risk-communication-and-intervention-to-reduce-exposure-and-to-minimize-the-health-effects-of-air-pollution, 2019.

Wierońska-Wiśniewska, F., Makowska, D., and Strugała, A.: Arsenic in polish coals: Content, mode of occurrence, and distribution during coal combustion process, Fuel, 312, https://doi.org/10.1016/j.fuel.2021.122992, 2022.

Xu, W., He, Y., Qiu, Y., Chen, C., Xie, C., Lei, L., Li, Z., Sun, J., Li, J., Fu, P., Wang, Z., Worsnop, D. R., and Sun, Y.: Mass spectral characterization of primary emissions and implications in source apportionment of organic aerosol, Atmos. Meas. Tech., 13(6), 3205–3219, https://doi.org/10.5194/amt-13-3205-2020, 2020.

Yang, S., Yuan, B., Peng, Y., Huang, S., Chen, W., Hu, W., Pei, C., Zhou, J., Parrish, D., Wang, W., He, X., Cheng, C., Li, X., Yang, X., Song, Y., Wang, H., Qi, J., Wang, B., Wang, C., Wang, C., Wang, Z., Li, T., Zheng, E., Wang, S., Wu, C., Cai1, M., Ye, C., Song, W., Cheng, P., Chen, D., Wang, X., Zhang, Z., Wang, X., Zheng, J., and Shao, M.: The formation and mitigation of nitrate pollution: comparison between urban and suburban environments, ACP, https://doi.org/10.5194/acp-22-4539, 2022.

Yuan, J., Lewis Modini, R., Zanatta, M., Herber, A. B., Müller, T., Wehner, B., Poulain, L., Tuch, T., Baltensperger, U., and Gysel-Beer, M.: Variability in the mass absorption cross section of black carbon (BC) aerosols is driven by BC internal mixing state at a central European background site (Melpitz, Germany) in winter, Atmos. Chem. Phys., 21(2), 635–655, https://doi.org/10.5194/acp-21-635-2021, 2021.

Yudovich, Y. E., and Ketris, M. P.: Chlorine in coal: A review, In International Journal of Coal Geology, 67, Issues 1–2, pp. 127–144, https://doi.org/10.1016/j.coal.2005.09.004, 2006.

Zhang, Q., Jimenez, J. L., Canagaratna, M. R., Ulbrich, I. M., Ng, N. L., Worsnop, D. R., and Sun, Y.: Understanding atmospheric organic aerosols via factor analysis of aerosol mass spectrometry: A review, In Analytical and Bioanalytical Chemistry, 401, Issue 10, pp. 3045–3067, https://doi.org/10.1007/s00216-011-5355-y, 2011.

1148 Zhang, Q., Rami Alfarra, M., Worsnop, D. R., Allan, J. D., Coe, H., Canagaratna, M. R., and Jimenez, J. L.:
1149   Deconvolution and quantification of hydrocarbon-like and oxygenated organic aerosols based on aerosol mass
1150   spectrometry, Environ. Sci. Technol., 39(13), 4938–4952, https://doi.org/10.1021/es048568l, 2005.

1151 Zhang, Y., Favez, O., Petit, J. E., Canonaco, F., Truong, F., Bonnaire, N., Crenn, V., Amodeo, T., Prévôt, A. S. H.,
1152   Sciare, J., Gros, V., and Albinet, A.: Six-year source apportionment of submicron organic aerosols from near-
1153   continuous highly time-resolved measurements at SIRTA (Paris area, France), Atmos. Chem. Phys., 19(23),
1154   14755–14776, https://doi.org/10.5194/acp-19-14755-2019, 2019.

1155 Zhang, Y. J., Tang, L. L., Wang, Z., Yu, H. X., Sun, Y. L., Liu, D., Qin, W., Canonaco, F., Prévôt, A. S. H., Zhang, H.
1156   L., and Zhou, H. C.: Insights into characteristics, sources, and evolution of submicron aerosols during harvest
1157   seasons in the Yangtze River delta region, China, Atmos. Chem. Phys., 15(3), 1331–1349,
1158   https://doi.org/10.5194/acp-15-1331-2015, 2015.

1159 Zhu, Q., Huang, X. F., Cao, L. M., Wei, L. T., Zhang, B., He, L. Y., Elser, M., Canonaco, F., Slowik, J. G., Bozzetti,
1160   C., El-Haddad, I., and Prévôt, A. S. H.: Improved source apportionment of organic aerosols in complex urban air
1161   pollution using the multilinear engine (ME-2), Atmos. Meas. Tech., 11(2), 1049–1060,
1162   https://doi.org/10.5194/amt-11-1049-2018, 2018.

1163

1164

1165
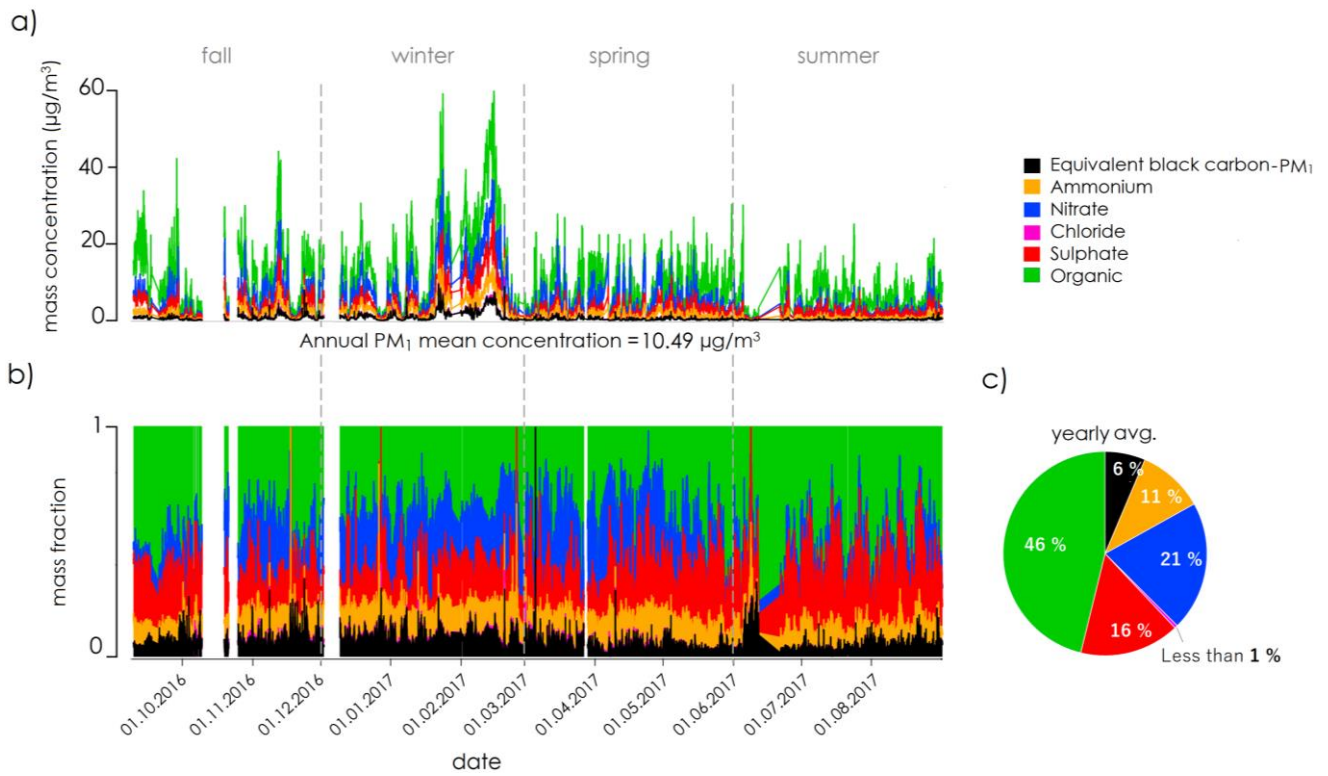
Fig. 1: Time series of a) the particulate PM$_1$ chemical composition, b) the corresponding mass fraction and c) average contribution of each chemical component (time is in UTC).
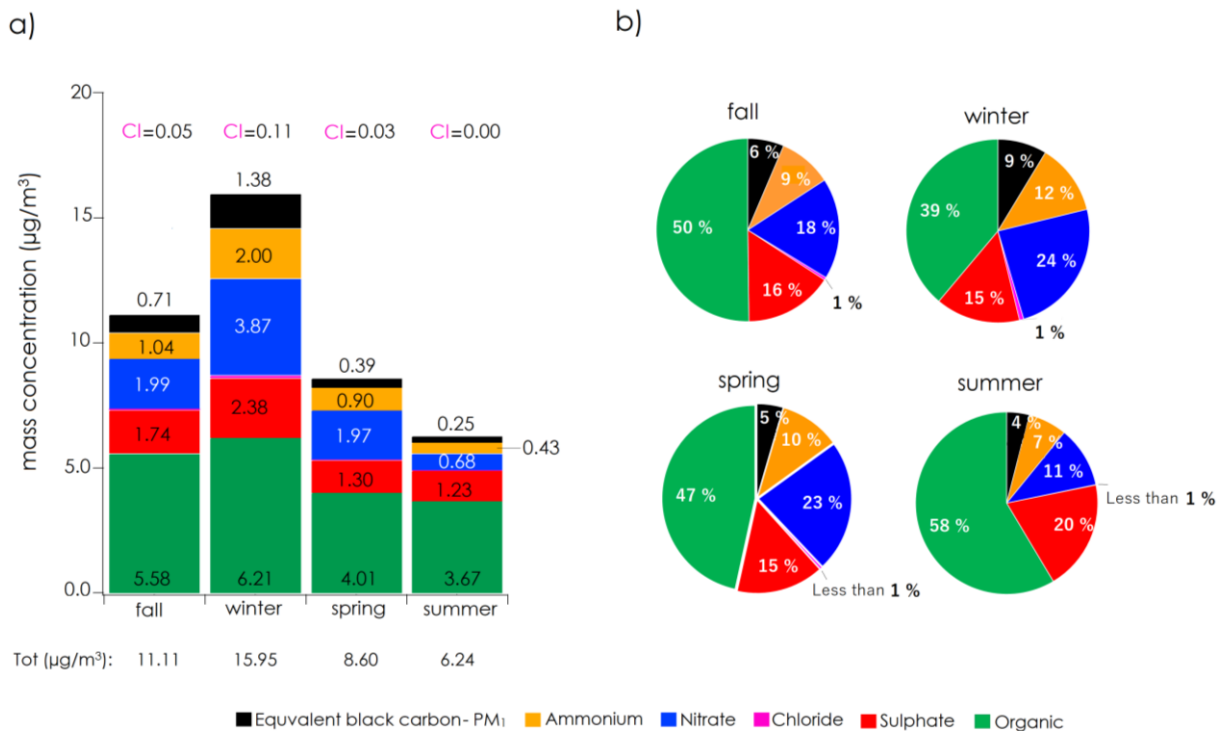
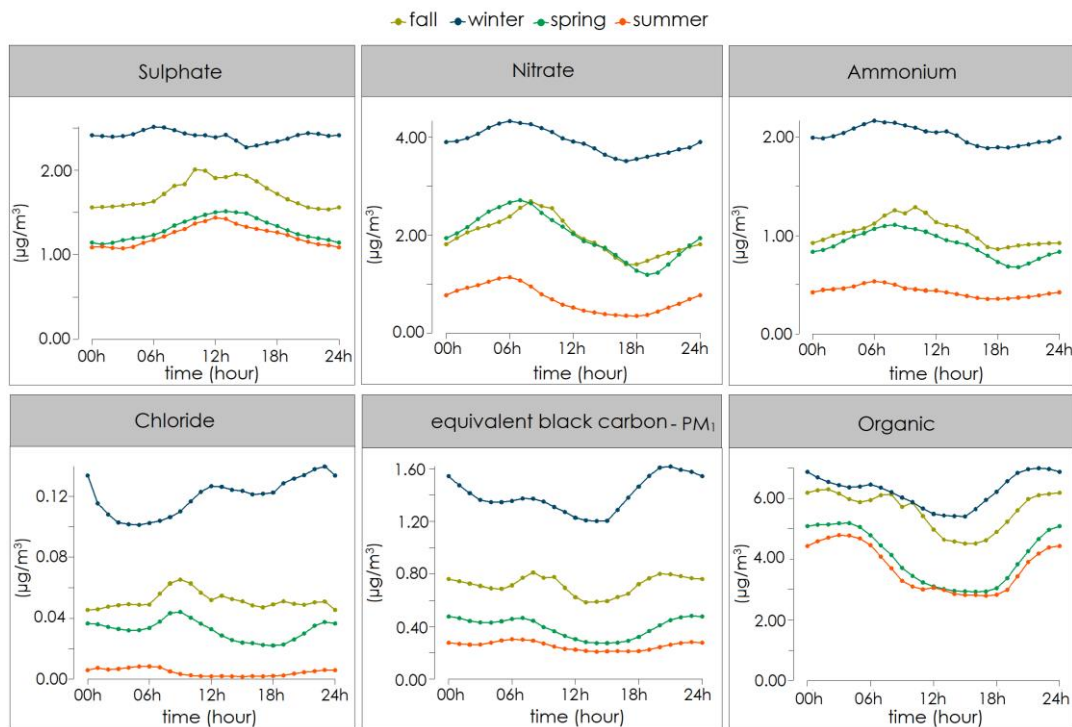**Fig. 2: seasonal variation of PM₁ a) absolute mass concentration and b) mass fraction.**

Fig. 3: Seasonal diurnal cycle of PM₁ for ACSM organic and inorganic species (time is in UTC).

38

1176 **Table. 1: Seasonal/yearly mass concentration of each ACSM species, each PMF factors, contribution of the different POA-PMF-**

1177 **eBC-PM$_1$, and correlation of each factors with related species; PM$_1$.**

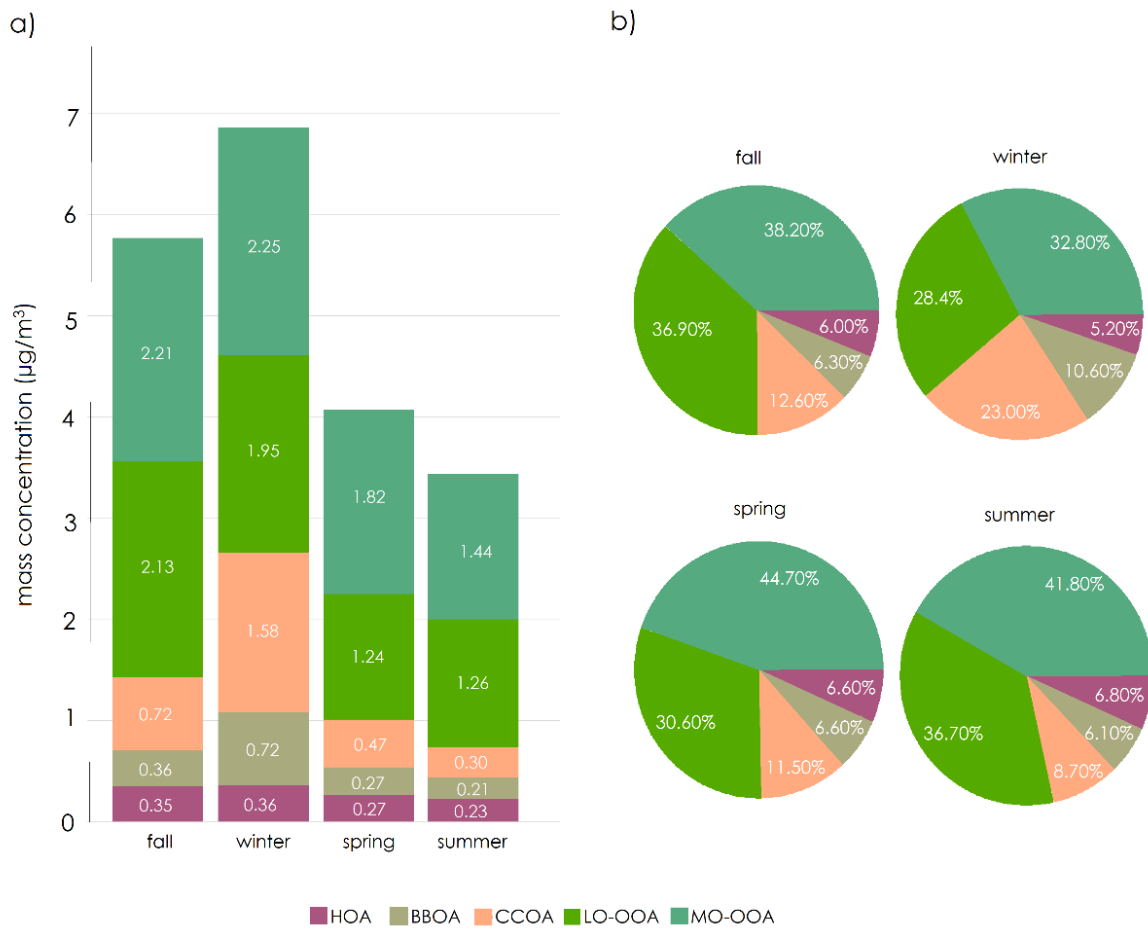| Species/ Factors		Fall	Winter	Spring	Summer	Yearly
ACSM **(μg/m^3)**	**Org**	5.58	6.21	4.01	3.67	4.84
	SO$_4^{2-}$	1.74	2.38	1.30	1.23	1.67
	NO$_3^-$	1.99	3.87	1.97	0.68	2.16
	NH$_4^+$	1.04	2.00	0.90	0.43	1.11
	Cl$^-$	0.05	0.11	0.03	0.00	0.05
MAAP **(μg/m^3)**	eBC -PM$_1$	0.71	1.38	0.39	0.25	0.66
PMF **(μg/m^3)**	**HOA**	0.35	0.36	0.27	0.23	0.30
	BBOA	0.36	0.72	0.27	0.21	0.39
	CCOA	0.72	1.58	0.47	0.30	0.77
	LO-OOA	2.13	1.95	1.24	1.26	1.62
	MO-OOA	2.21	2.25	1.82	1.44	1.92
eBC-PM$_1$ **(μg/m^3)**	eBC-PM$_1$-**HOA**	0.16	0.19	0.03	0.04	0.05
	eBC-PM$_1$-**BBOA**	0.34	0.38	0.17	0.15	0.25
	eBC-PM$_1$-**CCOA**	0.23	0.74	0.16	0.02	0.37
eBC-PM$_1$ **(%)**	eBC-PM$_1$-**HOA**	22	15	9	18	8
	eBC-PM$_1$-**BBOA**	47	29	47	69	37
	eBC-PM$_1$-**CCOA**	31	56	44	13	55
Correlation **(R^2)**	**HOA/** eBC-PM$_1$	0.49	0.52	0.34	0.24	0.33
	HOA/NO$_x$	0.23	0.12	0.32	0.23	0.17
	BBOA/Levo.	0.19	0.59	0.09	0.07	0.54
	BBOA/ eBC-PM$_1$	0.62	0.81	0.48	0.42	0.77
	CCOA/ eBC-PM$_1$	0.65	0.85	0.49	0.30	0.82
	CCOA/Cl$^-$	0.40	0.41	0.18	0.15	0.46
	LO-OOA/ NO$_3^-$	0.22	0.59	0.01	0.12	0.19
	LO-OOA/ SO$_4^2$	0.36	0.55	0.00	0.02	0.23
	MO-OOA / SO$_4^2$	0.58	0.47	0.34	0.42	0.44
	MO-OOA/ NO$_3^-$	0.24	0.47	0.16	0.24	0.31

1178
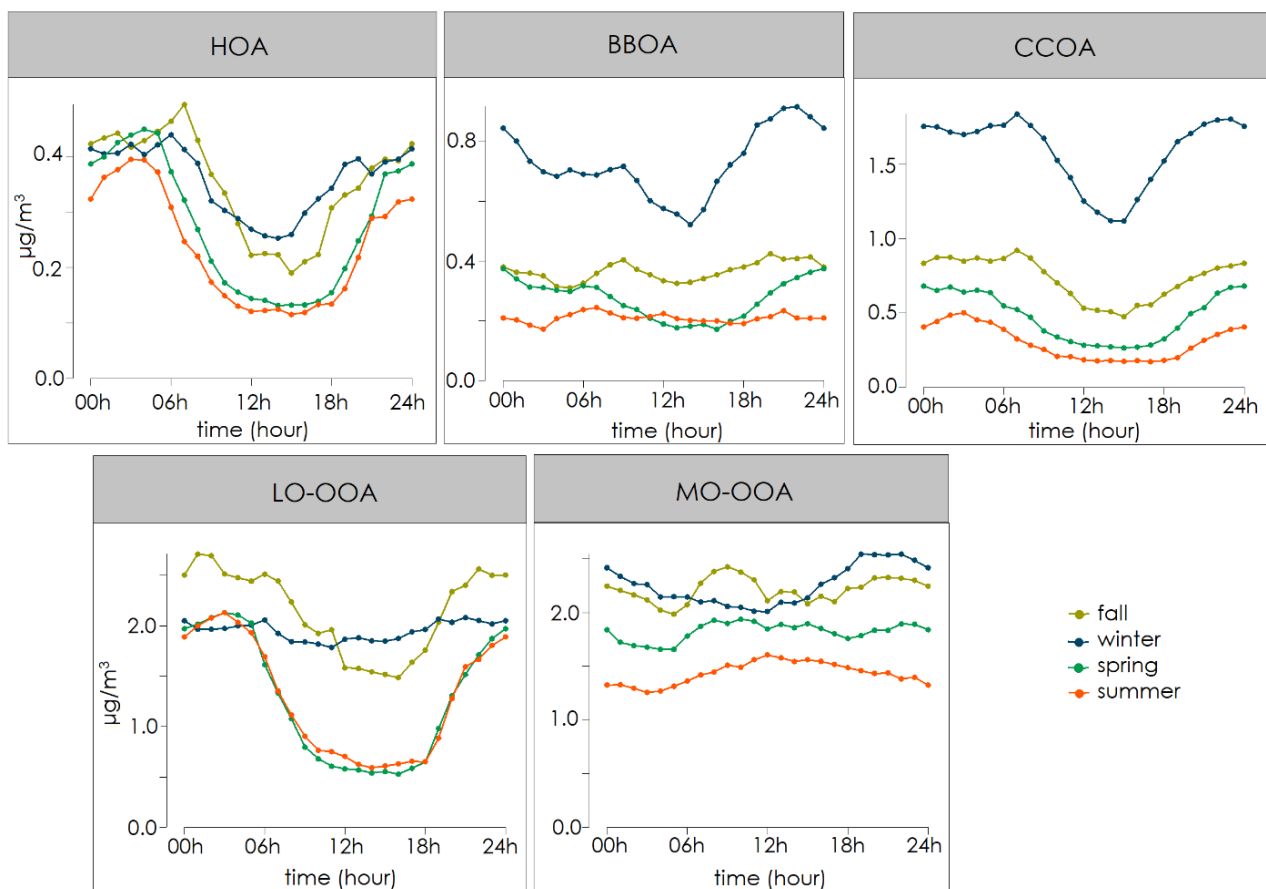1179
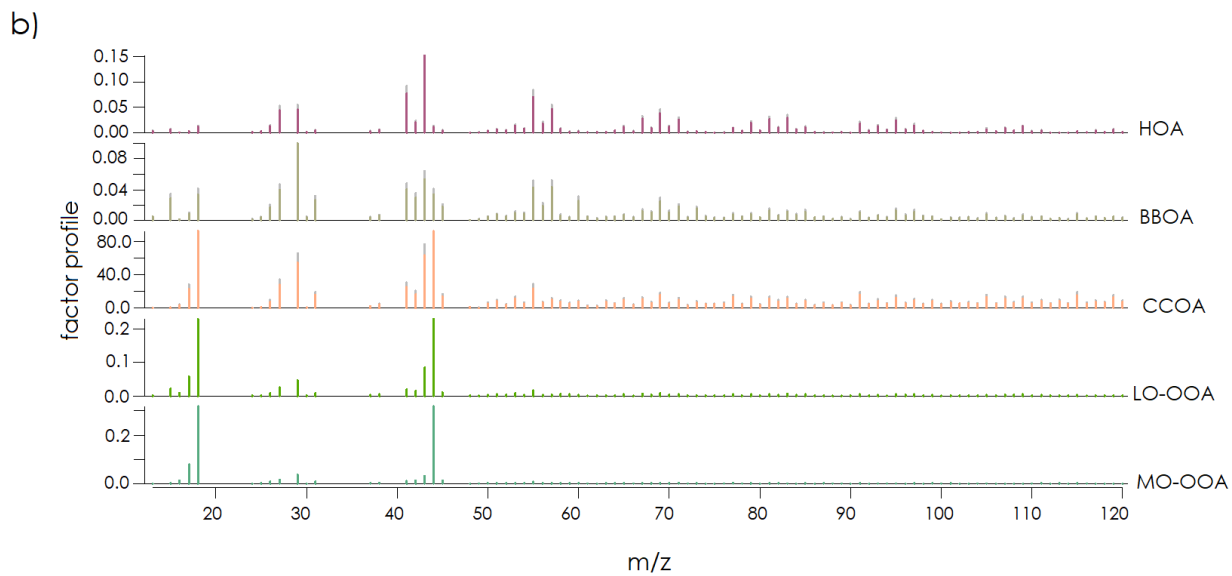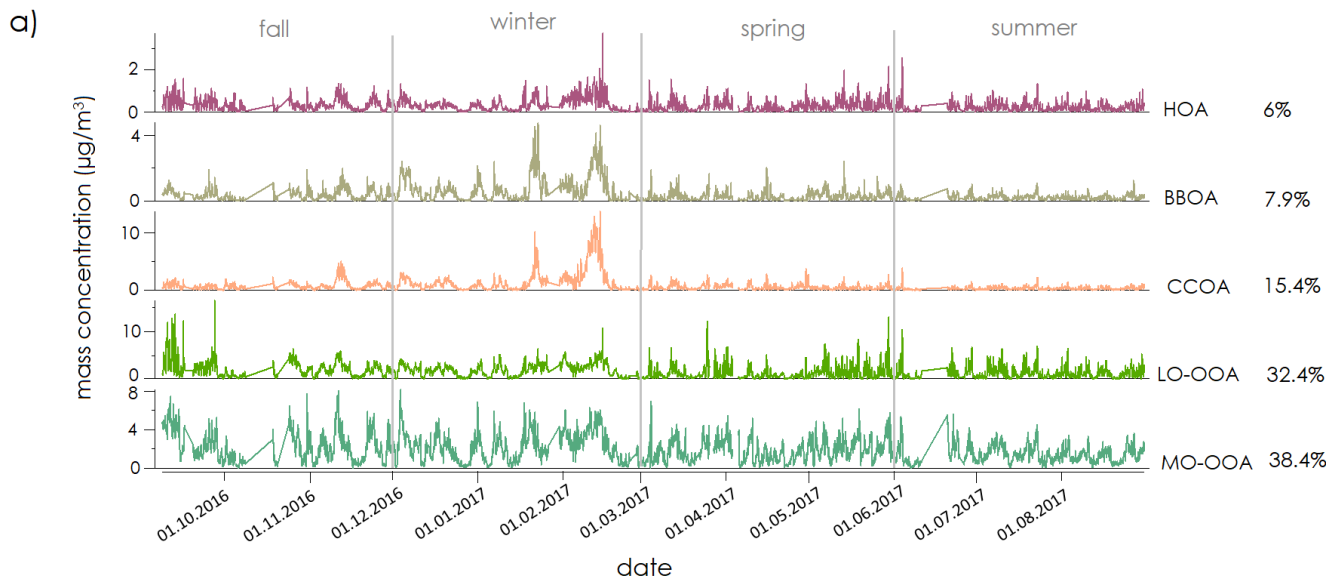
Fig. 4: Overview of averaged PMF (ME-2) results, a) time series, and b) mass spectral profile of organic PMF factors (time is in UTC).

a)

b)

fall

38.20%
6.00%
6.30%
12.60%
36.90%

winter

32.80%
5.20%
10.60%
23.00%
28.4%

spring

44.70%
6.60%
6.60%
11.50%
30.60%

summer

41.80%
6.80%
6.10%
8.70%
36.70%

■HOA ■BBOA ■CCOA ■LO-OOA ■MO-OOA

1184   **Fig. 5: Seasonal variation of a) mass concentration, b) mass fraction of PMF source factors.**

Fig. 6: Seasonal diurnal cycle (hourly averages) of the organic components HOA, BBOA, CCOA, LO-OOA and MO-OOA in UTC time.
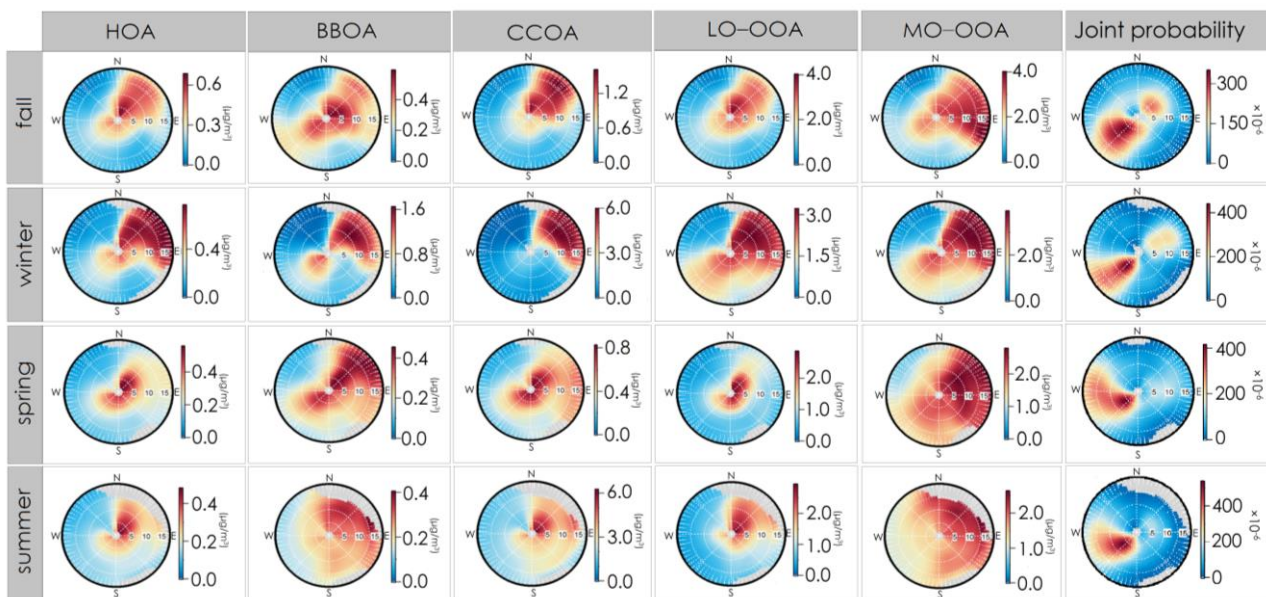
1189

1190 **Fig. 7: Seasonal NWR plots for the different PMF factors (in μg/m³).**

1191

a)

b)
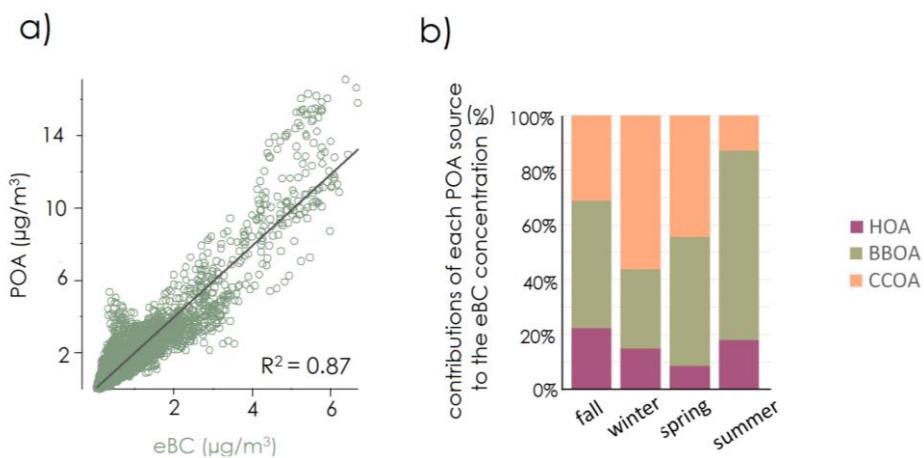
1192

1193 **Fig. 8: Contribution of the three POA factors to the mass concentration of** eBC-PM$_1$**, a) scatter plots POA vs** eBC-PM$_1$ **and b)**

1194 **contributions of sources to the eBC-PM$_1$ mass concentration.**

1195

1196
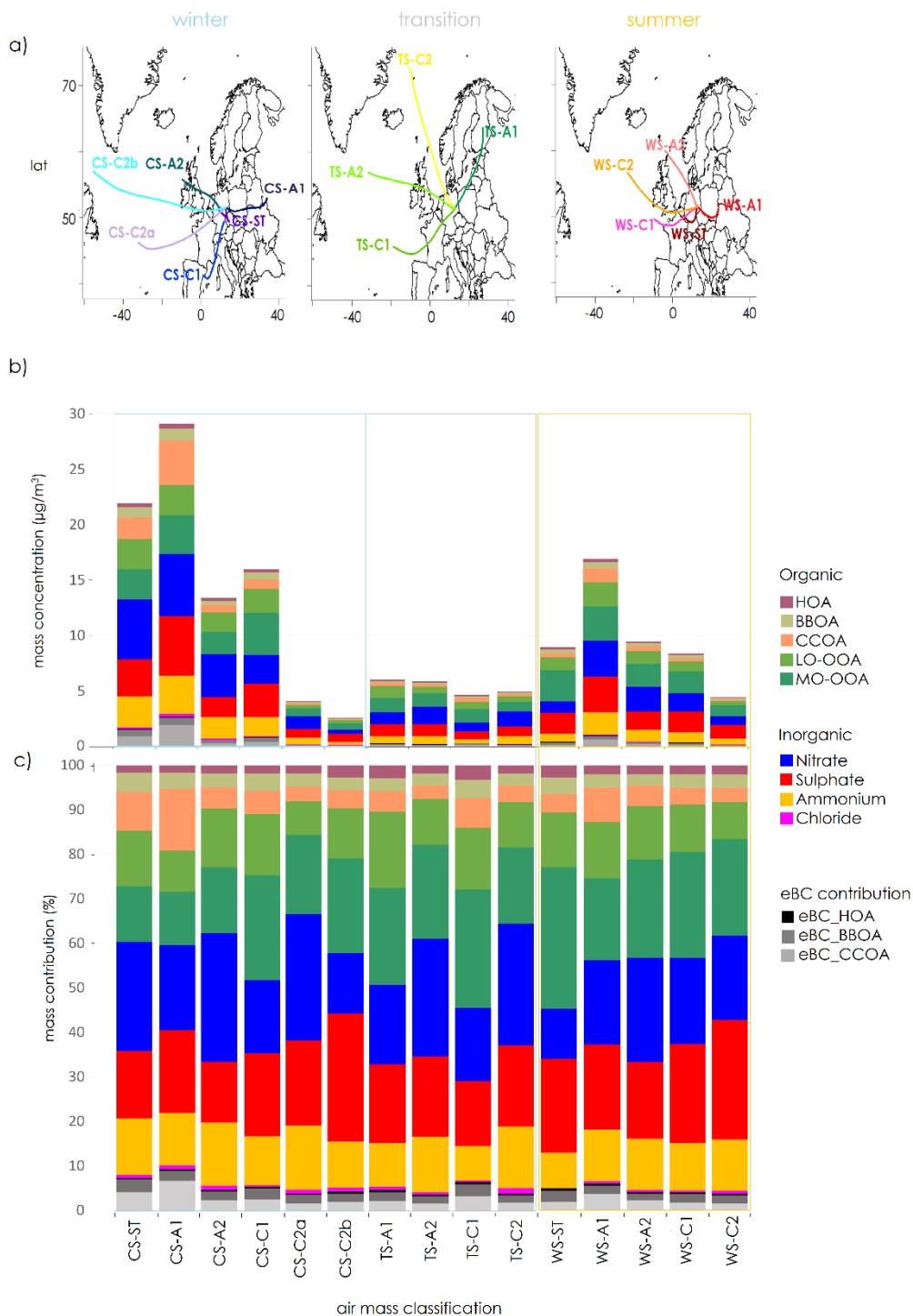
1197

Fig. 9: a) air mass classification based on one-year backward trajectories cluster analysis at 12:00 UTC, b) influence of air mass to

the PM$_1$ data and PMF factors, and c) contribution of them which averaged from 10:00 to 14:00 UTC.

1200

1201

1202

1203

1204 **Table. 2: Main statistical details of the 15 air mass types for total PM$_1$**

1205 **(CS=Cold Season, WS=Warm Season, ST=Stagnant, A=Anticyclonic, C=Cyclonic).**

Main season	Airmass type	Wind direction	Vorticity	Frequency (%)	Total mean (µg/m³)
Winter	CS-ST	Stagnating	Anticyclonic	14	21.95
	CS-A1	East	Anticyclonic	18	29.14
	CS-A2	West	Anticyclonic	8	13.39
	CS-C1	South	Cyclonic	10	15.99
	CS-C2a	South West	Cyclonic	3	04.09
	CS-C2b	West	Cyclonic	2	02.60
Transition (Spring/ Fall)	TS-A1	North East	Anticyclonic	4	06.06
	TS-A2	West	Anticyclonic	4	05.86
	TS-C1	South West	Cyclonic	3	04.69
	TS-C2	North West	Cyclonic	4	04.94
Summer	WS-ST	Stagnating	Anticyclonic	6	08.97
	WS-A1	South East	Anticyclonic	11	16.95
	WS-A2	North West	Anticyclonic	6	09.48
	WS-C1	West	Cyclonic	5	08.41
	WS-C2	West	Cyclonic	3	04.46

1206